Title

Constitutive activity of the dopamine receptor D5R, highly expressed in CA1 hippocampal neurons, selectively reduces $Ca_V3.2$ and $Ca_V3.3$ currents.

Running tittle

D5R constitutive activity reduces $Ca_V3.2$ and $Ca_V3.3$ currents.

Authors

[1]Emilio Román Mustafá; [1]Clara Inés McCarthy; [1]Andrea Estefanía Portales; [1,2]Santiago Cordisco Gonzalez; [1]Silvia Susana Rodríguez; and [1]Jesica Raingo.

Author's institutional affiliation

1-   Electrophysiology Laboratory of the Multidisciplinary Institute of Cell Biology [Argentine Research Council (CONICET), Scientific Research Commission of the Province of Buenos Aires (CIC-PBA) and National University of La Plata (UNLP)], Calle 526 S/N entre 10 y 11, 1900 La Plata, Buenos Aires, Argentina.

2-   Current address*: Unidad Ejecutora para el Estudio de las Neurociencias y Sistemas Complejos (ENyS), (CONICET), Buenos Aires, Argentina.*

The e-mail address, and telephone number(s) of the corresponding author

jraingo@gmail.com, +54 2214210112.

ORCID of the author(s)

Emilio Román Mustafá: https://orcid.org/0000-0001-7480-558X

Clara Inés McCarthy: https://orcid.org/0000-0002-6959-8552

Andrea Estefanía Portales: https://orcid.org/0000-0001-8645-633X

Santiago Cordisco Gonzalez: https://orcid.org/0000-0002-1318-7842

Silvia Susana Rodríguez: https://orcid.org/0000-0002-2546-0359

Jesica Raingo: https://orcid.org/0000-0002-2307-0373

Word count: 5075

Availability of data

The data that support the findings of this study are available from the corresponding author upon reasonable request.

Abstract (250 words)

Background and purpose: Ca$_V$3.1-3 currents differentially contribute to neuronal firing patterns. Ca$_V$3 are regulated by G protein-coupled receptors (GPCRs) activity, but information about Ca$_V$3 as targets of the constitutive activity of GPCRs is scarce. Our aim is to investigate the impact of D5R constitutive activity, a GPCR with high levels of basal activity, on Ca$_V$3 functionality. D5R and Ca$_V$3 are expressed in the hippocampus and both have been independently linked to pathophysiological states associated with epilepsy.

Experimental approach: our study models were HEK293T cells heterologously expressing D1R or D5R and Ca$_V$3.1-3, and mouse brain slices containing the hippocampus. We used chlorpromazine (CPZ, D1R/D5R inverse agonist) and a D5R mutant lacking constitutive activity as experimental tools. We measured Ca$_V$3 currents and excitability parameters using the *patch-clamp* technique. We completed our study with computational modeling and imaging technique.

Key results: we found a higher sensitivity to TTA-P2 (Ca$_V$3 blocker) in CA1 pyramidal neurons obtained from CPZ-treated animals compared to vehicle-treated animals. We found that Ca$_V$3.2 and Ca$_V$3.3 –but not Ca$_V$3.1– are targets of D5R constitutive activity in HEK293T cells. Finally, we found an increased firing rate in CA1 pyramidal neurons from CPZ-treated animals in comparison with vehicle-treated animals. Similar changes in firing rate were observed on a neuronal model with controlled Ca$_V$3 currents levels.

Conclusions and Implications: native hippocampal Ca$_V$3 and recombinant Ca$_V$3.2-3 are sensitive to D5R constitutive activity. Manipulation of D5R constitutive activity could be a valuable strategy to control neuronal excitability, especially in exacerbated conditions such as epilepsy.

Key words

Main text

1- Introduction

Low-voltage-activated calcium channels (Ca$_V$3) are important proteins underlying neuronal activity since their opening induces the depolarization of the plasma membrane (PM) and control firing pattern (Ertel et al., 2000; Tsien, 1983). Ca$_V$3 family comprises the Ca$_V$3.1, Ca$_V$3.2 and Ca$_V$3.3 subtypes which generate currents with different kinetic properties. Current traces indicate that Ca$_V$3.1 and Cav3.2 activate and inactivate faster in comparison with Ca$_V$3.3 (Klockner et al., 1999; Monteil, Chemin, Bourinet, et al., 2000; Monteil, Chemin, Leuranguer, et al., 2000; Perez-Reyes, 2003). The specific contribution of each Ca$_V$3 subtype to define the firing pattern in a certain brain nucleus is hard to establish with pharmacological tools. Despite the development of blockers with high selectivity for Ca$_V$3, such as TTA-A2 and TTA-P2 (Choe et al., 2011; Kraus et al., 2010), no natural or synthetic compounds have been identified to specifically target Ca$_V$3 subtypes (Snutch & Zamponi, 2018; Weiss & Zamponi, 2019a, 2019b). In this context, *in silico* simulations of neuronal behavior are useful to predict how each Ca$_V$3 subtype impacts on the firing pattern (Chemin et al., 2002).

G protein-coupled receptors (GPCRs) are key modulators of Ca$_V$ in neurons (Dolphin, 2003; Proft & Weiss, 2015; Y. Zhang, Jiang, Snutch, & Tao, 2013). Here we focus on the study of the modulation of Ca$_V$3 by the D1R-like subfamily of dopamine receptors (D1R and D5R) which have high constitutive activity and play a critical role in neuronal excitability (Demchyshyn, McConkey, & Niznik, 2000; Tiberi & Caron, 1994; B. Zhang, Albaker, Plouffe, Lefebvre, & Tiberi, 2014). The constitutive activity, defined as the intrinsic ability of a GPCR to signal in the absence of ligands (Gainetdinov, Premont, Bohn, Lefkowitz, & Caron, 2004), might provide a basal activity level that could function as a mechanism of long-lasting neuronal regulation. In this regard, the effect of ligand-evoked GPCR activity on Ca$_V$ has been extensively studied (Dolphin, 2003; Proft & Weiss, 2015; Y. Zhang et al., 2013). In the last ten years, our group has reported the impact of the constitutive activity of several GPCRs on Ca$_V$2 and its impact on synaptic transmission

(Agosti et al., 2017; Cordisco Gonzalez, Mustafa, Rodriguez, Perello, & Raingo, 2020; Lopez Soto et al., 2015; Martinez Damonte, Rodriguez, & Raingo, 2018; McCarthy et al., 2020; Mustafa et al., 2021; Mustafa et al., 2017). The physiological functions of D1R and D5R have not yet been differentiated due to the lack of selective ligands for each receptor subtype (Nichols, 2010). However, *in vitro* studies show significant differences between these two receptors: (1) D5R exhibits higher levels of constitutive activity compared to D1R, (2) D5R shows increased potency and affinity for dopamine, and (3) D5R couples to both Gs and Gq proteins, while D1R only couples to Gs protein (Sahu, Tyeryar, Vongtau, Sibley, & Undieh, 2009; Tiberi & Caron, 1994; B. Zhang et al., 2014). Interestingly several reports show that Ca_V3 are targeted by Gq-coupled GPCRs (Hildebrand et al., 2007; Mustafa, Cordisco Gonzalez, & Raingo, 2020). Therefore, the D1R/D5R constitutive activity could likely impact on Ca_V3 functionality.

There are several experimental approaches to manipulate the levels of GPCR constitutive activity. A simple *in vitro* strategy is the use of increasing concentrations of the GPCR-containing plasmid in the transfection mix since it is expected that the levels of constitutive activity positively correlate with the amount GPCR expressed (Agosti et al., 2017; Cordisco Gonzalez et al., 2020; Lopez Soto et al., 2015; Martinez Damonte et al., 2018; McCarthy et al., 2020; Tiberi & Caron, 1994). Moreover, GPCR-mutants lacking basal activity that preserve the ability to respond their ligands are valuable tools to isolate the effects of constitutive activity from those of ligand-evoked (Al-Fulaij, Ren, Beinborn, & Kopin, 2008; Pantel et al., 2006; Rojo, McCarthy, Raingo, & Rubinstein, 2020; Torz et al., 2020). Finally, the binding of inverse agonists reduces the constitutively active levels of a GPCR (Costa & Cotecchia, 2005). In particular for D1R/D5R it has been reported that some typical and atypical antipsychotics such as chlorpromazine (CPZ), flupenthixol and clozapine function as inverse agonists (Paz, Stahl, Rela, Murer, & Tubert, 2022; B. Zhang et al., 2014). In this line, we previously used CPZ to manipulate the constitutive activity of D1R/D5R in the prefrontal cortex (McCarthy et al., 2020).

Here we hypothesize that the constitutive activities of D1R and D5R differentially regulate the density and/or functionality of $Ca_V3.1$-3 in hippocampus, controlling neuronal intrinsic properties and excitability. Hippocampal Ca_V3 have a crucial role in the pathophysiology of epilepsy (Becker et al., 2008). All Ca_V3 subtypes are expressed in the hippocampus: in the dentate gyrus the expression levels of the three Ca_V3 subtypes is similar, however, in the CA1 area $Ca_V3.2$ and $Ca_V3.3$ have a higher expression than $Ca_V3.1$ (Aguado, Garcia-Madrona, Gil-Minguez, & Lujan, 2016; Yunker et al., 2003). In this regard, the increased density of Ca_V3 in CA1 neurons from animal models of epilepsy would explain great part of the change from the regular to the burst firing pattern (Sanabria, Su, & Yaari,

2001). On the other hand, the activation of D1R/D5R in the hippocampus has a pro-seizure effect due to increased neuronal excitability (Bozzi & Borrelli, 2013). The expression of D5R is high in the CA1 and the dentate gyrus regions, but low in the CA3 region, at the same time that the expression of D1R is slight in the three areas (Megat et al., 2018; Sarinana, Kitamura, Kunzler, Sultzman, & Tonegawa, 2014; Sasamori et al., 2022). Here we present data showing that CPZ, a D1R/D5R inverse agonist, increases the Ca$_V$3 currents in hippocampal CA1 pyramidal neurons and consequently modifies neuronal excitability. Moreover, we demonstrated that D5R and D1R coexpression specifically reduces Ca$_V$3.2 and Ca$_V$3.3 current. We focused our study on D5R effect and we confirmed the role of its constitutive activity on Ca$_V$3 current inhibition and studied the properties of this modulation in a heterologous expression system.

2- Methods

2.1 - Cell culture and transient transfection

HEK293T (ECACC Cat# 96121229, RRID: CVCL_2737) cells were grown in Dulbecco's modified Eagle's medium (DMEM; Gibco) with 10 % fetal bovine serum (FBS; Internegocios) and split at 80 % confluence. Cells were transfected with plasmids containing voltage-gated calcium channel subunit Ca$_V$3.1 (CACNA1G, GenBank access no. AF190860), Ca$_V$3.2-GFP (CACNA1H, GenBank access no. NM021098) or Ca$_V$3.3 (CACNA1I, GenBank access NM_021096), with or without D5R (D5R, GenBank access NM_000798.5) or D5R mutant version (D5RST1), or D1R (D1R, GenBank access NM_000794). We generated D5R-mCherry encoding plasmid to perform imaging experiments (for details see below). To identify transfected cells, an eGFP (enhanced green fluorescent protein)-containing plasmid was used. Transfections were done using Lipofectamine 2000 (Invitrogen) and Opti-MEM (Gibco). When needed, empty pcDNA3.1 (+) was cotransfected to maintain the same amount of DNA between conditions.

Lipofectamine was used according to the manufacturer's specifications. Transfected cells were cultured for 48 h to allow Ca$_V$3 expression. On the day of the experiment, cells were detached from the culture disk with 0.25 mg/mL trypsin (Microvet), rinsed twice and kept at room temperature (23 °C) in DMEM.

Ca$_V$3.1 clone was obtained from AddGene (#45811); Ca$_V$3.2-GFP clone was a gift from Dr. E. Bourinet (Institut de Génomique Fonctionnelle, Université de Montpellier, Montpellier, France); and Ca$_V$3.3 clone was provided by Dr. D. Lipscombe (Brown University, Providence, RI, USA). D1R, D5R and D5RST1 clones were provided by Dr. M. Tiberi (University of Ottawa, Ottawa, ON, Canada).

2.2- Generation of D5R-mCherry construct

Plasmid containing cDNAs encoding wild-type D5R (pCMV5-hD5R) was kindly provided by Dr. Tiberi and mCh-Sec61 beta was a purchased from Addgene (#49155, a gift from Gia Voeltz). To generate the D5R-mCherry construct the sequence without stop codons was amplified by PCR from pCMV5-hD5R with a forward oligonucleotide that amplifies upstream to the BclI restriction site (D5-Fw: 5' AGCCTGCGCGCTTCCATCAA 3') and a reverse oligonucleotide without stop codon containing a linker sequence (D5 linker – Rv: 5' *GGTGGCGACCGGTGGATCCCGGGC*ATGGAATCCATTCGGGGTGAAAGGTGTTA 3', *italic* sequence correspond to the linker sequence). mCherry sequence was amplified by PCR from mCh-Sec61 beta with a forward oligonucleotide containing a linker sequence (mCh linker-Fw: 5' *GCCCGGGATCCACCGGTCGCCACC*GCTAGCATGGTGAGCAAGGGCGAGGAG 3', *italic* sequence correspond to the linker sequence) and an reverse oligonucleotide containing a stop codon upstream to the HindIII restriction site (mCh-Rv: 5' CCC*AAGCTT*TCACTTGTACAGCTCGTCCATG 3', *italic* sequence correspond to the HindIII restriction site). An overlapping PCR reaction (excluding primers) was used to generate the full-length fusion genes with the linker sequence of both primary fragments generated above. Next, a final PCR step with primers D5-Fw and mCh-Rv was used to amplify the full-length fusion product and this PCR fragment was digested with BclI and HindIII enzymes to be inserted into the BclI and HindIII sites of pCMV5 -hD5R. The fidelity of the construct was confirmed by full-length sequencing of the coding region by Macrogen.

2.3- Drugs

Chlorpromazine as commercial antipsychotic drug (chlorpromazine HCl, 25 mg/ml injectable blister, CAS #50–53-3; Laboratorios Duncan S.A.) was donated by Dr. Martinez Mónaco and Dr. Pinedo (Italian Hospital of La Plata, Buenos Aires, Argentina) and used for intraperitoneal (i.p.) injections in mice and 44-h preincubations of HEK293T transfected cells. CPZ stock solution was stored at room temperature, protected from light, and dissolved in saline solution 0.9 % NaCl < 24 h before i.p. injections. For patch clamp experiments from mouse hippocampal slices, the sodium channel blocker tetrodotoxin (1 µM; CAS #4368–28-9, #T8024; Sigma-Aldrich), the Ca_V3 blocker TTA-P2 (1 µM; CAS # T-155, Alomone Labs) were used. The drug dopamine hydrochloride (CAS #62–31-7, #H8502; Sigma-Aldrich) was used in patch clamp experiments in HEK293T cells.

2.4- Animals and ethical approval

Pathogen free C57BL/6 wild-type (WT) mice of both sexes were housed in a 12 h light–dark cycle in a climate-controlled room (22 °C) at the IMBICE animal facility. Animals

had *ad libitum* access to water and standard rodent chow. This study was performed in strict accordance with the recommendations of the Guide for the Care and Use of Laboratory Animals of the National Research Council. Animal suffering was minimized. All experimentation received approval from the Institutional Animal Care and Use Committee of the IMBICE. Animal studies are reported in compliance with ARRIVE 2.0 guideline (Percie du Sert et al., 2020).

2.5- Animal treatment and hippocampal slice preparations

For this study a total of 14 mice (vehicle, N = 8; chlorpromazine-treated, N = 6) were used. WT mice 4–6-wk-old of both sexes counterbalanced were treated with vehicle (saline solution NaCl 0.9 %) or chlorpromazine (1 mg/kg) through two i.p. injections (0.1 ml/10 g) 24 h and 1 h before sacrifice. Mice were anaesthetized with isoflurane (2 %) and immediately decapitated. Brains were quickly removed and hippocampal horizontal brain slices (300 µm) containing the hippocampus (Bischofberger, Engel, Li, Geiger, & Jonas, 2006; Xiong, Metheny, Johnson, & Cohen, 2017) were prepared in bubble ice-cold 95 % O_2–5 % CO_2-equilibrated solution containing (in mM): 110 choline chloride, 25 glucose, 25 $NaHCO_3$, 7 $MgCl_2$, 11.6 ascorbic acid, 3.1 sodium pyruvate, 2.5 KCl, 1.25 NaH_2PO_4 and 0.5 $CaCl_2$, pH 7.4. Brain slices were obtained using a vibratory tissue slicer (PELCO easiSlicer; #11000; Ted Pella Inc.) and then transferred to an incubation chamber filled with 95 % O_2, 5 % CO_2–equilibrated artificial cerebrospinal fluid (aCSF) containing (in mM) 124 NaCl, 26.2 $NaHCO_3$, 11 glucose, 2.5 KCl, 2.5 $CaCl_2$, 1.3 $MgCl_2$, and 1 NaH_2PO_4, pH 7.4, with HCl. Slices were maintained at 37 °C for 20 min and left to recover at room temperature ($\sim$ 24 °C) for 30 min before recordings.

2.6- Electrophysiology

Axopatch 200 amplifier (Molecular Devices) was used for patch-clamp experiments in HEK293T cells, which were all in whole-cell and voltage- -clamp configuration. Data were sampled at 20 kHz and filtered at 10 kHz (-3 dB) using PCLAMP8.2 software (Molecular Devices). Patch clamp recordings in brain slices were made with an EPC7 (HEKA Electronik) amplifier in whole-cell and voltage- -clamp configuration, and data were sampled at 20 kHz and filtered at 10 kHz (−3dB) using PatchMaster (HEKA Electronik) software. Recording pipettes with resistances between 2 and 4 MΩ were used and filled with internal solution. Series resistances of less than 6 MΩ were admitted and compensated 80 % with a 10 µs lag time. We discarded cells with a leak current higher than 100 pA at holding potential and leak current was subtracted online using a P/-4 protocol. We perfused solutions from a 10 ml syringe containing bath solution placed 30 cm over the patch clamp chamber so the gravity drives the liquid to the chamber. The flow rate was regulated at 1 ml/min with a valve.

The perfusion inlet attaches several three-way stopcocks for delivering different solutions to the chamber. Control, dopamine, chlorpromazine, tetrodotoxin and TTA-P2 containing solutions were applied with this system connected to different ports of the stopcocks. The liquid junction potential between the internal and the external solution containing 10 mM $BaCl_2$ solution (see below) was ~ 6.5 mV. These values were measured before experiments and non-corrected thus all voltages showed were slightly more negative. All recordings were obtained at room temperature (~ 24 °C).

- *Barium currents of transiently transfected HEK293T cells:* external solution contained (in mM): 10 $BaCl_2$, 1 $MgCl_2$, 10 HEPES, 140 TEA-chloride and 6 CsCl (pH 7.4 with CsOH).

The test-pulse protocol consisted in square pulses applied from -100 to -20 mV for $Ca_V3.1$, $Ca_V3.2$, and $Ca_V3.3$, for 200 ms every 10 s. The voltage dependence of activation of total Cav3 currents showed in figure 5 B was determined by measuring the peak of the Ca_V3 current in response to 200 ms depolarizing steps from -90 mV to +40 mV in 10 mV increments from a holding membrane potential of −100 mV. For steady-state inactivation experiments the protocol consisted in step depolarizations to -20 mV preceded by 2 s prepulse to a potential ranging from -120 to +20 mV in 10 mV increments from a holding potential of -100 mV in control condition. For experiments shown in figure 8 we used a train of action potential from a CA1 hippocampal neuron as voltage stimuli previously used in (Castiglioni, Raingo, & Lipscombe, 2006).

-*Native calcium currents of CA1 pyramidal neurons:* hippocampal horizontal mouse brain slices were transferred to the recording chamber and visualized with an upright Zeiss Examiner. A1 microscope (#491404–0001-000), a digital camera (Rolera Bolt Scientific CMOS; QImaging), and Micro-Manager 1.4 open-source microscopy software (Vale Lab, University of California, San Francisco, USA). Whole-cell patch-clamp recordings in voltage clamp mode were conducted at room temperature (~ 24 °C) in the previously described aCSF (2.5 mM Ca^{2+}) under a continuous flow rate of 2.5 ml/min. Recording electrodes with resistances between 3 and 6 MΩ were used and filled with internal solution containing (in mM) 115 Cs-methanesulfonate, 20 tetraethylammonium chloride, 10 CsCl, 5 NaCl, 10 HEPES, 10 EGTA, 4 Mg-ATP, and 0.3 Na-GTP, pH 7.4, with CsOH. For native calcium current recordings, tetrodotoxin (1 µM) was added to normal aCSF (2.5 mM Ca^{2+}) to block native voltage-gated sodium channels. Neurons were held at resting potential (−70 mV), and native calcium currents were evoked applying square pulses from −90 to -30 mV or to 0 mV (200-ms duration). Additionally, the specific Ca_V3 blocker TTA-P2 (1 µM) was added to analyze Ca_V3 contributions to total native calcium currents.

-Current-clamp recording of CA1 pyramidal neurons: Neurons from CA1 region of hippocampal horizontal slices were visualized as described above. Whole-cell patch-clamp recordings in current clamp mode were conducted at room temperature ($\sim$ 24 °C) in the previously described aCSF under a continuous flow rate of 2.5 ml/min. Recording pipettes with resistances between 3 and 6 MΩ were filled with an internal solution containing the following (in mM): 140 K-gluconate, 5 KCl, 5 NaCl, 10 HEPES, 0.6 EGTA, 4 MgCl$_2$, 3 Na$_2$-ATP, and 0.3 Na$_2$GTP (pH 7.3 with KOH). Neurons were held at -70 mV between sweeps. Square current steps from -80 pA to 200 pA were applied to evoke action potentials (5 pA increase, 400 ms duration). The specific Ca$_V$3 blocker TTA-P2 (1 µM) was added to analyze Ca$_V$3 contributions to the firing response.

2.7- Imaging

For imaging experiments cells were plated on 12 mm diameter glasses covered with poli-D-lysine (Sigma, 0.1 mg/mL) and transfected after 24 h with Ca$_V$3.2-GFP alone or plus the receptor plasmid (D5R or D5RST1) at the specified molar ratio. For experiments shown in figure 7B we preincubated two conditions (with or without D5R expression) with CPZ (1µM). After 48 h, cells were prepared for image acquisition. Briefly, cells were washed with phosphate buffered-saline (PBS, pH = 7.4) and incubated for 1 min with CellMask solution (ThermoFisher, 1:2000 in DMEM) for cell membrane staining. Afterwards, cells were washed with PBS and incubated with 2 % paraformaldehyde in PBS for 10 min for fixation. Finally, cells were washed with PBS and mounted on glass slides with mounting media containing Höescht. Fluorescent images were acquired with a Zeiss AxioObserver D1 equipped with an Apotome.2 structured illumination module and an AxioCam 506 monochrome camera.

-Quantification of GFP percentage in the plasma membrane (PM): to determine percentage of GFP in the PM a region of interest (ROI) delimiting the cell surface was drawn according to the CellMask signal. The outer edge of the PM was hand-drawn and subsequently used to automatically determine the inner edge in a selection located 0.4 µm from the outer edge towards the center of the cell. The ROI delimiting the PM was then transferred to the green channel and the integrated fluorescence intensity (IFI) was measured in the area inside the outer and inner edges of the PM. To calculate the quantity of GFP in the PM the inner IFI was subtracted to the outer IFI. Finally, the quantity of GFP in the PM was expressed as a percentage of the total GFP in the cell (outer IFI). Image visualization, PM delimitation and fluorescence measurements were made with the open-source software Fiji (Schindelin et al., 2012).

-Quantification of mCherry signal (determination of D5R expression): to determine D5R wild type cellular expression, the D5R wild type gene was fused to mCherry fluorescent protein as we described above. HEK293T cells were transfected with Ca$_V$3.3 and

D5RmCherry at 1, 0.5 and 0.1 D5RmCherry:Ca$_V$3.3 molar ratios. 48 post-transfection cells were washed with PBS, fixed with 4 % paraformaldehyde, washed again and mounted on glass slides. Fluorescent images were acquired with a Zeiss AxioObserver D1 equipped with an Apotome.2 structured illumination module and an AxioCam 506 monochrome camera. To quantify D5RmCherry cell expression the open source program Fiji was used (Schindelin et al., 2012). Briefly, cells were delimited following mCherry signal and added to ROI manager. Finally, we measured the fluorescence (sum of pixel values) inside the cellular ROI.

2.8- Modelling

Simulations of CA1 pyramidal neurons behavior were performed using the NEURON simulation environment (Hines & Carnevale, 1997). We used the multicompartment model configuration of regular behavior described by (Uebachs et al., 2010) (Accession number: 125152, available on Yale University (https://senselab.med.yale.edu/ModelDB/)).

To emulate our data in presence of D5R, we reduced the native Ca$_V$3 current conductance (named CaT in the model) was multiplied by 0.38. Conversely, to emulate the CPZ-treatment the CaT current was multiplied by 1.68. Firing frequency was determined using PCLAMP10.7 software (Molecular Devices). The membrane potential was recorded from the virtual soma during 500 ms injecting from 0.0 to 1.0 nA of current by steps of 0.1 nA.

2.9- Statistics

Data were analyzed and visualized using the OriginPro 9 (Origin-Lab) and GraphPad Prism 6 (GraphPad Software, Inc.) software. To determine outliers in our data, we used the ROUT method (based on the False Discovery Rate (FDR)) offered by GraphPad Prism 6. We used Kolmogorov–Smirnov to test for conformity to a normal distribution, and variance homogeneity was examined using Bartlett's (normally distributed data) and Brown-Forsythe´s (non-normally distributed data) test. *P* values were calculated from one- or two-sample Student´s *t* tests (normally distributed data) or Mann–Whitney test (non-normally distributed data), and multiple comparison one way- ANOVA with Tukey's post-test (normally distributed data). In same experiments we used a Wilcoxon matched-pairs signed rank test to estimate P values. We used Extra-sum square F-test to compare different data function fits. The specific statistical test used is indicated for each data set in the figure legend. Data were expressed as mean ± SEM.

3.0- Nomenclature of Targets and Ligands

Key protein targets and ligands in this article are hyperlinked to corresponding entries in http://www.guidetopharmacology.org, and are permanently archived in the Concise Guide

to PHARMACOLOGY 2021/22 (AlexanderChristopoulos, et al., 2021; Alexander, Mathie, et al., 2021).

3- Results

3.1- Chronic treatment with the D1R/D5R inverse agonist chlorpromazine increases the native Ca$_V$3 currents in CA1 pyramidal neurons from hippocampus.

To manipulate the D1R/D5R constitutive activity we performed intraperitoneal injections in mice with the inverse agonist chlorpromazine (CPZ, 1 mg/kg). We recorded Ca$_V$ currents from CA1 pyramidal neurons using a square stimulus from a resting potential of -90 mV to -30 (where we expect a greater contribution of the Ca$_V$3 to the total Ca$_V$ current (Kortekaas & Wadman, 1997)) and we observed an increased amplitude in the Ca$_V$ current recorded in slices from CPZ-treated animals compared to vehicle. In contrast, we failed to observe differences in the levels of Ca$_V$ current evoked by a stimulus from -90 mv to 0 mV (where a higher contribution of high-activated-voltage Ca$_V$ to the total calcium current is expected (Kortekaas & Wadman, 1997). We calculated the ratio between the amplitude of the Ca$_V$ recorded at -30 mV and 0 mV for each neuron, obtaining a larger value in CPZ-treated animals in comparison with vehicle (figure 1A). Next, to determinate the specific contribution of the Ca$_V$3 channels to the total current we applied the Ca$_V$3 blocker, 1 µM TTA-P2 (Choe et al., 2011), and we found an increased Ca$_V$ inhibition in slices from CPZ-treated mice in comparison with slices obtained from vehicle-treated animals at -30 mV but not at 0 mV (figure 1B). Thus, our results allow us to conclude that the chronic treatment with CPZ increases the Ca$_V$3 native currents in hippocampal CA1 pyramidal neurons possibly by reducing the D1R/D5R constitutive activity.

3.2- D5R coexpression selectively reduces the macroscopic current of two Ca$_V$3 subtypes (Ca$_V$3.2 and Ca$_V$3.3)

Based on the strong effect observed for CPZ on Ca$_V$3 currents recorded in hippocampal CA1 pyramidal neurons we next explored the effect of D5R and D1R constitutive activity on Ca$_V$3 currents in HEK293T cells transfected separately with the three Ca$_V$3 subtypes. To this aim we measured the Ca$_V$ macroscopic current in presence of increasing relative amounts of D5R and D1R in transfected HEK293T cells (different molar ratios among D1R/D5R and Ca$_V$3 plasmids in the transfection cDNA mix). As we show in figure 2, the coexpression of increasing amounts of D5R-containing plasmid fails to modify the amplitude of Ca$_V$3.1 macroscopic current (figure 2A), while significantly reducing Cav3.2 and Ca$_V$3.3 macroscopic currents (figure 2B and 2C). We repeated these experiments with D1R and found a strong reduction of Ca$_V$3.3 basal current due to D1R coexpression, while

Ca$_V$3.1 remains insensitive and Ca$_V$3.2 seems to be less sensitive to D1R than to D5R (supplementary figure 1). Moreover, we ran an experimental control for D5R, measured the changes in fluorescence signal of mCherry tagged D5R at the same conditions at which we measured the currents (D5R: Ca$_V$3.3 molar ratio and cDNA amounts) and we found that there is a correlation between the signal intensity and cDNA amount (supplementary figure 2), as we had previously proven for D1R (McCarthy et al., 2020). Furthermore, we show that the acute application of dopamine (10 µM) has a mild but significant inhibitory effect on the macroscopic calcium current in HEK293T cells coexpressing Ca$_V$3.1, Ca$_V$3.2 or Ca$_V$3.3 and a low amount of D5R containing plasmid (0.1 D5R:Ca$_V$3 molar ratio) (figure 2D, E and F). We used a low amount of receptor for these experiments because a high level of basal current is required to observe an acute effect of dopamine. On the other hand, in cells expressing D1R (0.1 D1R:Ca$_V$3 molar ratio) dopamine application reduces only the Ca$_V$3.1 current by 20% while Ca$_V$3.2 and Ca$_V$3.3 currents remain insensitive (supplementary figure 1D, E and F). Finally we run a control experiment applying dopamine (10 µM) on cells expressing only Ca$_V$3.2 and found no effect (I$_{Ca_V3.2}$ inhibition by dopamine (%) = -2.10 ± 1.05, P= 0.103 vs 0, N = 6, one sample Student's t test). These results indicate that the sole coexpression of D5R selectively reduces Ca$_V$3.2 and Ca$_V$3.3 macroscopic currents without a significant effect on Ca$_V$3.1. We found a similar effect when coexpressing D1R. Moreover, dopamine acute application slightly inhibits the three Ca$_V$3 subtypes in cells expressing D5R, while for D1R we observed a selective effect on Ca$_V$3.1. Considering the high expression of D5R on CA1 area (Megat et al., 2018; Sarinana et al., 2014; Sasamori et al., 2022) we investigated the properties of basal Ca$_V$3 modulation by this particular D1R-like subtype.

3.3- D5R constitutive activity selectively reduces Ca$_V$3.2 and Ca$_V$3.3 macroscopic currents.

In order to determine if the chronic reduction on Ca$_V$3.2 and Ca$_V$3.3 macroscopic currents by D5R coexpression is due to its constitutive activity (B. Zhang et al., 2014) we used a genetic tool: a mutant lacking basal activity (D5RST1) (B. Zhang, Yang, & Tiberi, 2015). We tested Ca$_V$3.2 and Ca$_V$3.3 functionality in presence of D5RST1. Since it has been previously reported that the membrane expression of D5RST1 is reduced by 50 % compared to the wild-type version of this receptor (B. Zhang et al., 2015), here we used a Ca$_V$3.2: wild-type D5R molar ratio of 0.5 and Ca$_V$3.2: D5RST1 of 1 in order to avoid misinterpretation of data due to a lower expression level of the D5ST1. Figure 3 shows that the levels of Ca$_V$3.2 and Ca$_V$3.3 currents in HEK293T cells coexpressing Ca$_V$3.2 or Ca$_V$3.3 and D5RST1 are not significantly different from the control levels (we replaced D5R or D5RST1 by empty plasmid), while the coexpression of wild-type D5R significantly reduces the basal Ca$_V$3.2

(figure 3A) and Ca$_V$3.3 (figure 3B) currents. Thus, we can conclude that D5R constitutive activity chronically inhibits the Ca$_V$3.2 and Ca$_V$3.3 macroscopic currents.

3.4- The reduction in Ca$_V$3.2 and Ca$_V$3.3 basal currents by D5R constitutive activity is occluded by chronic preincubation with CPZ.

Next we manipulated the D5R constitutive activity by using the inverse agonist CPZ and explored the effect of CPZ chronic treatment on HEK293T cells coexpressing D5R and Ca$_V$3.2 or Ca$_V$3.3. Figure 4 shows that in HEK293T cells coexpressing D5R and Ca$_V$3.2 (figure 4A) or Ca$_V$3.3 (figure 4B), at a 1 D5R: Ca$_V$3 molar ratio, preincubation with CPZ (1 µM) for 24 or 44 hours restores Ca$_V$ currents to levels similar to control conditions (HEK293T cells expressing Ca$_V$3.2 or Ca$_V$3.3 and empty plasmid). Importantly, we observed that CPZ fails to modify Ca$_V$3.2 or Ca$_V$3.3 basal current in absence of D5R (figure 4). As a control we also assayed the effect of chronic 44 hours application of CPZ (1 µM) on HEK293T cells expressing Ca$_V$3.1 and we failed to observe a significant modulation of the macroscopic current (supplementary figure 3). Simultaneously, we discarded a direct stimulatory effect of CPZ on Ca$_V$3 channels by observing the lack of significant current changes after acute application of CPZ (1 µM) on HEK293T cells only expressing Ca$_V$3.2, Ca$_V$3.3 (figure 4C and 4D) and Ca$_V$3.1 (supplementary figure 3). We conclude that chronic treatment with CPZ occludes the reduction in Ca$_V$3.2 and Ca$_V$3.3 basal currents induced by D5R constitutive activity *in vitro*. Moreover, our results allow us to discard a direct effect of CPZ on the three Ca$_V$3 subtypes.

3.5- D5R constitutive activity reduces the Ca$_V$3 current resultant of coexpressing Ca$_V$3.1, Ca$_V$3.2 and Ca$_V$3.3 on HEK293T cells.

Next we explored the impact of D5R constitutive activity on Ca$_V$3 current of HEK293T cells simultaneously expressing the three Ca$_V$3 subtypes to investigate if the D5R inhibitory effect on isolated Ca$_V$3.2 and Ca$_V$3.3 affects the resultant Ca$_V$3 current. Figure 5A illustrates the representative Ca$_V$ traces obtained in a HEK293T cell coexpressing Ca$_V$3.1-3 in the presence or not of D5R. We observed that the coexpression of D5R partially but significantly reduces the resultant Ca$_V$3 current amplitude, as expected if D5R constitutive activity targets two of the three Ca$_V$3 subtypes. We next investigated changes in biophysical parameters that could contribute to the macroscopic basal Ca$_V$3 current reduction seen in HEK293T cells coexpressing Ca$_V$3.1-3 and D5R. We generated current–voltage (I–V) curves in cells coexpressing Ca$_V$3.1-3 with or without D5R and found that the resultant Ca$_V$3 current was significantly reduced by D5R coexpression at a wide range of voltages (from − 30 to 20 mV). We additionally compared the fit parameters of the I–V curves and observed that D5R coexpression causes a significant reduction of the maximum conductance (G$_{max}$) of Ca$_V$3

current without changes in the half activation voltage ($V_{1/2}$), the reversal potential (V_{rev}) or the slope of activation (K) (figure 5B). We only determined the biophysical parameters of cells coexpressing D5R where a basal Ca$_V$3 current was measurable. This reduction in G_{max} could be due to changes in the number of channels available to be open, the single channel conductance and/or open probability (Hille, 1992). Moreover, we tested if D5R modulates the voltage dependency of Ca$_V$3 activation and /or inactivation as a function of the voltage by building G/G_{max}-V curves (figure 5C) and performing experiments of steady-state inactivation to build I/I_{max}-V curves (figure 5D). We found no differences in the fitting parameters obtained from these curves between HEK293T cells coexpressing D5R and control (see tables on figure 5C and 5D). On the other hand, we analyzed the activation and inactivation kinetics of the resultant Ca$_V$3 current in the presence or not of D5R. In control conditions we observed an intermediate behavior in comparison to the kinetics observed for each isolated Ca$_V$3 channel and D5R coexpression failed to modify the activation and inactivation time constants of resultant Ca$_V$3 current (figure 5E and 5F). The set of results shown here indicate that the D5R constitutive activity reduces the macroscopic current in cells simultaneously expressing the three Ca$_V$3 subtypes, a likely scenario for hippocampal neurons, through a reduction in the G_{max} without appreciable modifications in activation- or inactivation- voltage dependency or kinetic properties.

3.6- D5R constitutive activity reduces resultant Ca$_V$3, Ca$_V$3.2 and Ca$_V$3.3 gating currents

Since we found a reduction on the G_{max} for Ca$_V$3 with D5R coexpression, we decided to explore if such effect is the result of impairment in the number of Ca$_V$ channels available to open. Thus, we measured Ca$_V$3 gating current as an estimation of the number of functional channels on the PM (Karmazinova, Baumgart, Perez-Reyes, & Lacinova, 2011; Karmazinova, Jaskova, Griac, Perez-Reyes, & Lacinova, 2015). We recorded the Ca$_V$3 ON gating currents from a holding potential of -100 mV to the reversal potential estimated for each cell assayed (from ~ 40 to ~ 50 mV) in cells coexpressing Ca$_V$3.1-3 with or without D5R. Figure 6A shows that D5R coexpression reduces the resultant Ca$_V$3 gating current charge moved (Q_{rev}) normalized by the capacitance. We also tested, in independent experiments, if the D5R constitutive activity impacts on Ca$_V$3.2 and Ca$_V$3.3 gating currents, and we observed that the coexpression of D5R significantly reduces the Ca$_V$3.2 and Ca$_V$3.3 gating charge moved (figure 6B and 6C). Thus, we could postulate that the reduction in macroscopic Ca$_V$3.2 and Ca$_V$3.3 basal currents is caused by the impact of the D5R constitutive activity on the number of Ca$_V$ available to open. Nevertheless, with our experiments we cannot rule out a possible effect at the intrinsic channel properties.

3.7- D5R constitutive activity reduces the $Ca_V3.2$-GFP surface density

Taking advantage of an available version of $Ca_V3.2$ tagged with GFP ($Ca_V3.2$-GFP) we further explored if D5R coexpression reduces the localization of $Ca_V3.2$ on the PM by performing imaging experiments. We delimitated the cell surface using a commercial PM marker (CellMask). Figure 7A shows that the percentage of green fluorescent signal from $Ca_V3.2$-GFP on the PM was proportionally and significantly reduced by the increasing amount of D5R expressed on HEK293T cells. We also show that the GFP signal on the PM in HEK293T cells coexpressing D5RST1 was similar to control (in absence of D5R expression). Additionally, figure 7B shows that in HEK293T cells coexpressing D5R and $Ca_V3.2$-GFP at a 1 D5R: Ca_V3 molar ratio preincubation with CPZ (1 µM) for 44 hours restores the percentage of green fluorescent signal from $Ca_V3.2$-GFP on the PM to levels similar to control conditions (HEK293T cells expressing $Ca_V3.2$ and empty plasmid). We also demonstrate that the GFP signal on the PM was not affected for the preincubation of CPZ in HEK293T cells solely expressing Cav3.2-GFP. Overall, data from figures 5, 6 and 7 allow us to suggest that D5R constitutive activity chronically inhibits $Ca_V3.2$ –and likely $Ca_V3.3$– macroscopic currents by reducing the density of channels on the cell surface.

3.8- D5R constitutive activity reduces Ca_V3 currents induced by CA1 action potential waveforms.

A question that arose based on the results obtained was: does the $Ca_V3.2$-3 basal current reduction mediated by D5R constitutive activity persist in response to a physiological electrical stimulus? To answer this question, we recorded Ca_V3 currents stimulated by a train of action potentials originally obtained from CA1 hippocampal neurons, in HEK293T coexpressing the three Ca_V3 subtypes with or without D5R. We chose this stimulation paradigm because the CA1 neurons are known to express the three Ca_V isoform and the D5R (Aguado et al., 2016; McKay et al., 2006; Megat et al., 2018; Sarinana et al., 2014; Sasamori et al., 2022; Yunker et al., 2003). Figure 8A displays the results showing that Ca_V3 currents are significantly reduced in cells coexpressing D5R at each single stimulus in comparison with control. Moreover, we examined the behavior of peak currents during the train of action potentials and found a peak current depression with stimulus number in HEK293T solely expressing $Ca_V3.1$ or $Ca_V3.2$, whereas for HEK293T cells expressing the $Ca_V3.3$ subtype we observed a current facilitation under the same train of stimulus as it has been described before (Chemin et al., 2002) (figure 8B and 8C). Accordingly, cells coexpressing the three Ca_V3 subtypes displayed a depression in the current but this was less profound than for $Ca_V3.2$ or $Ca_V3.3$ alone, and the D5R constitutive activity further increased this depression (figure 8C). Thus, D5R constitutive activity profoundly impacts on

resultant Ca$_V$3 current behavior obtained using a physiological voltage stimulus. Moreover the remaining current in presence of D5R is consistent with a lower contribution of Ca$_V$3.2 and Ca$_V$3.3 to the total Ca$_V$3 current.

3.9- Chronic treatment with the D1R/D5R inverse agonist chlorpromazine increases the firing rate in hippocampal CA1 pyramidal neurons

Next, we evaluated the impact of the modulation of Ca$_V$3 by D1R/D5R constitutive activity on neuronal excitability. We performed current clamp experiments on pyramidal CA1 neurons in brain slices from animals previously treated with CPZ or vehicle, with or without acute application of TTA-P2 (1 µM). Figure 9A shows representative traces of voltage responses to increasing injected current and mean values of the number of spikes versus injected current. We found a significantly higher number of spikes at a given current stimulus (from 40 to 80 pA) in neurons from animals treated with CPZ compared to vehicle. In addition, the application of TTA-P2 significantly reduces the number of spikes in neurons from animals treated with CPZ (from 40 to 140 pA) compared to vehicle (figure 9A). We also observed that the rheobase was lower in CPZ-treated condition compared to vehicle, and the application of TTA-P2 increases the rheobase only in neurons from CPZ-treated animals (CPZ (pA) = 35.83 ± 10.52 (N = 6) and CPZ + TTA-P2 (pA) = 99.17 ± 26.22 (N = 6), P = 0.0313; vehicle (pA) = 95.87 ± 14.68 (N = 4) and vehicle +TTA-P2 (pA) = 133.9 ± 19.35 (N = 4), P = 0.2500, Wilcoxon matched-pairs signed rank test). On the other hand, resting membrane potential, input resistance and action potential threshold remained unchanged by the treatment with CPZ (figure 9B). Finally, we quantified action potential parameters (RMP (resting membrane potential), V$_{thre}$ (threshold membrane potential), V$_{repolarization}$ (repolarization membrane potential), V$_{max}$ (maximal voltage peak of the action potential), max. rise slope (maximum rise slope) and min. decay slope (minimum decay slope)) in neurons from animals treated or not with vehicle or CPZ and we failed to find significant differences between conditions (see table on figure 9C). Those values were obtained from phase plot analysis of the first action potential (injected current 0.14 nA). Therefore, our results suggest that the reduction of Ca$_V$3 current by D1R/D5R constitutive activity would reduce the firing rate and increase the rheobase in CA1 hippocampal neurons.

3.10 Manipulating Ca$_V$3 current levels modulates the firing rate in an *in silico* model of hippocampal CA1 pyramidal neuron

Finally, in order to predict and confirm the impact of D5R constitutive activity on neurons we used a simulation software to model action potentials firing. We specifically used the software NEURON for hippocampal CA1 pyramidal neurons previously published (Uebachs et al., 2010). Since we observed a 62 % reduction of the Ca$_V$3 G$_{max}$ in HEK293T

cells expressing D5R (figure 5), we simulated the effect of D5R constitutive activity on the firing frequency by reducing to 38 % of the Ca_V3 conductance current (named CaT) in the model. We conserved all the other values included on the equation describing the activation (m_∞) and steady-state inactivation (h_∞) curves and the equations for the voltage dependency of the activation (Tau_m) and inactivation (Tau_h) time constants because we failed to observe significant effects on these parameters in our experiments (figure 5). In agreement with data shown in figure 9, we observed a reduction in the number of spikes evoked by increasing current stimuli when we emulated D5R overexpression in comparison with a neuron with 100 % of Ca_V3 current (figure 10). Conversely, we simulated the CPZ treatment on neuronal excitability. For this purpose, we relied on our data displayed in figure 1 (showing a 68 % increase on the Ca_V3 sensitivity to TTA-P2 in animals previously injected with CPZ), and we multiplied the Ca_V3 conductance by 1.68 in the neuronal model. Figure 10 shows that there is an increase in the firing frequency of action potentials in neuron with 168 % of Ca_V3. Taken together, our data suggest that the modulation of Ca_V3 current density in CA1 hippocampal neurons by D5R constitutive activity could have a great impact on neuronal electrical activity.

4- Discussion

Our present data support the presence of a chronic inhibitory effect of D1R/D5R constitutive activity on Ca_V3 currents in hippocampal neurons from the CA1 region. Moreover, in transfected HEK293T cells, we identified the specific Ca_V3 isoforms sensitive to both D1R or D5R coexpression and agonist-evoked activity. We investigated the features of D5R constitutive activity mediated inhibition of $Ca_V3.2$-3 current because is the most abundantly expressed D1R-like subtype in the CA1 region (Megat et al., 2018; Sarinana et al., 2014; Sasamori et al., 2022).

We used a pharmacological approach to reduce the D1R/D5R constitutive activity. We chose chlorpromazine, one member of the antipsychotic drug group with proven effect as inverse agonist of D1R and D5R (Cai, Gurdal, Smith, Wang, & Friedman, 1999; McCarthy et al., 2020; B. Zhang et al., 2014). We found that CPZ occludes the inhibitory effect of D5R on $Ca_V3.2$-3 currents in HEK293T cells at two incubation times, with 24 hours being enough to see a significant effect, and we further confirmed our results by assaying the effect of a mutant of D5R lacking constitutive activity (B. Zhang et al., 2015). In agreement with these observations, CPZ increases the Ca_V3 component in pyramidal neurons from hippocampal CA1, an area with high D5R expression (Megat et al., 2018; Sarinana et al., 2014; Sasamori et al., 2022). Based on our data from supplementary figure 1 showing that D1R coexpression reduces $Ca_V3.3$ and likely $Ca_V3.2$, CPZ could also be acting on D1R reducing

its constitutive activity and further increasing Ca_V3 current. In this line, a recent publication showed the impact of clozapine and flupenthixol, other reported D1R/D5R inverse agonists, on the electrical activity of striatal cholinergic interneurons in an animal model of dyskinesia (Paz et al., 2022). Moreover, the treatment with flupenthixol changes the firing pattern from a pathological burst to a physiological tonic firing in subthalamic nucleus (Chetrit et al., 2013). These reports reinforce the idea of using antipsychotic drugs as inverse agonist to modulate the constitutive activity of D1R/D5R receptors. Endogenous inverse agonists have been discovered for two constitutive active GPCRs while for D1R/D5R they are still unknown. In this regard, we previously showed that the endogenous inverse agonists AgRP (Agouti-related protein) and LEAP2 (liver-expressed antimicrobial peptide 2) strongly impact of on the functionality of Ca_V through a reduction of the constitutive activity of MC4R (melanocortin-4 receptor) and GHSR1a (growth hormone secretagogue receptor type 1a), respectively (Agosti et al., 2017; Barrile et al., 2019; Mustafa et al., 2021). We propose that the reduction in Ca_V3 currents by D5R basal activity constitutes a chronic form of inhibition that could be overcome by synthetic inverse agonists and by still unidentified endogenous ligands.

Here we found that $Ca_V3.2$-3 are chronically inhibited by D5R constitutive activity while $Ca_V3.1$ remains insensitive. On the other hand, the acute dopamine mediated activation of D5R mildly inhibits all three Ca_V3 subtypes. Mechanism of biased signaling in GPCRs could be one possible explanation for the differential effect of D5R on Ca_V3 currents between these two activation modes of D5R (Conroy, Free, & Sibley, 2015; Wootten, Christopoulos, Marti-Solano, Babu, & Sexton, 2018). Moreover, these channel subtypes could have features that shape their sensitivity to a given signaling cascade. In this regard, other reports using *in vitro* models described Ca_V3 isoform specificity by GPCR activity: (1) muscarinic M1R- and GHSR1a ligand-evoked activities acutely reduce $Ca_V3.3$ current, but has no effect on $Ca_V3.1$ and $Ca_V3.2$ (Hildebrand et al., 2007; Mustafa et al., 2020); (2) corticotrophin releasing factor receptor 1 (CRFR1)- and neurokinin 1 receptor (NK1R)-activation solely inhibit $Ca_V3.2$ current (Rangel, Sanchez-Armass, & Meza, 2010; You, Altier, & Zamponi, 2010), (3) G-protein $\beta_2\gamma_2$ reduces $Ca_V3.2$ macroscopic currents without affecting the $Ca_V3.1$ subtype (Wolfe, Wang, Howard, Garrison, & Barrett, 2003), among others. Since these three channels are widely expressed across the nervous system and their gating properties are markedly different, efforts have been done to isolate their currents without success (Weiss & Zamponi, 2019a, 2019b). Previous studies *in vitro* and the recent resolution of $Ca_V3.1$ and $Ca_V3.3$ structures could illuminate that pursuit (He et al., 2022; Zhao et al., 2019). Here we found a physiological mechanism that could favor the relative contribution of $Ca_V3.1$ in D5R-expressing neurons. This seems to be the case in CA1

neurons since we found that TTA-P2 has a larger effect on these neurons when animals were treated with CPZ. $Ca_V3.1$ is a fast activating and inactivating conductance with a marked depression when stimulated by action potential waveforms that could contribute to burst firing (Yunker et al., 2003). Thus, our data and others suggest that changing the contribution of Ca_V3 specific subtypes to the total current could be a common mechanism of GPCRs to tune the electrical activity in neurons.

We found that the basal inhibitory effect of D5R on $Ca_V3.2$ and $Ca_V3.3$ currents is related to a decrease of channel density in the membrane. We observed a reduction in the gating charge moved for both channels, after examining that none of the gating properties are significantly changed, and a decrease in the percentage of GFP signal located at the cells surface -that is occluded by CPZ treatment- using a GFP-tagged $Ca_V3.2$ version in HEK293T expressing D5R. Changes in channel trafficking is a recurrent observation for the effect of the constitutive activity of GPCRs on Ca_V (Kisilevsky et al., 2008; Lopez Soto et al., 2015; McCarthy et al., 2020; Mustafa et al., 2017), however there is no common mechanism mediating these changes. In the case of GHSR1a constitutive activity, the presence of $Ca_V\beta$ auxiliary subunit is required (Mustafa et al., 2017), while in the case of stimulation of $Ca_V2.2$ by D1R in the prefrontal cortex a physical interaction between the channel and constitutively active D1R is necessary (Kisilevsky et al., 2008; McCarthy et al., 2020). On the other hand, a diminished density of channels on cell surface has been described for some variants of $Ca_V3.2$ and $Ca_V3.3$ associated with pathophysiological conditions such as amyotrophic lateral sclerosis and schizophrenia (Andrade et al., 2016; Stringer et al., 2020), respectively. Therefore, the density of Ca_V3 available on the cell surface is highly prone to regulatory mechanisms.

Due to the diverse gating properties of Ca_V3 isoforms and the complex changes occurring in neuronal membrane potential it is hard to predict how the D5R constitutive activity can impact native Ca_V3 current and the consequent effect on membrane potential. Here we used a simplified strategy to predict the Ca_V3 behavior in neurons: we evaluated the effect of D5R coexpression on Ca_V3 currents in HEK293T cells expressing the three Ca_V3 subtypes. This approach resembles the one used to study resultant $Ca_V3.2$ and $Ca_V1.2$ current sensitive to small GTPase Rem in HEK293T cells (Finlin, Crump, Satin, & Andres, 2003). We found that the reduction in Ca_V3 currents by D5R coexpression in not complete as expected considering that the $Ca_V3.1$ expressed in these cells is insensitive to this modulation. We investigated at gating properties changes and found that only G_{max} seems to be affected, in agreement with the changes in membrane channel density and gating charge moved. Regarding the Ca_V3 kinetic, we found that both activation and inactivation kinetics

are intermediate between the fast changes observed for $Ca_V3.1$ and $Ca_V3.2$ and the slower behavior described for $Ca_V3.3$. In the presence of D5R the total current is reduced but the gating and kinetics parameters remain unchanged. This last result was unexpected as we reasoned that the kinetic of the remaining current would be somewhat faster. Nevertheless, our results highlight the importance of assaying a modulatory effect on the combination of sensitive and insensitive conductances in order to approximate the conditions to the physiological context.

Another feature that is difficult to predict is the behavior of this combination of channels under more physiological voltage stimuli such as action potential waveforms. Related to this, a previous report showed that several typical action potential voltage stimuli exacerbates the differences between two $Ca_V2.2$ spliced isoform observed by using square stimuli (Castiglioni et al., 2006). Under these conditions, using action potential waveforms as stimuli, $Ca_V3.3$ displays lower current levels when expressed alone in comparison with $Ca_V3.1$ and $Ca_V3.2$, possibly due to its slow activation kinetic. Thus, it is plausible that the contribution of this D5R-sensitive channel is minor when the three channels are coexpressed in this condition. It is known that $Ca_V3.1$ and $Ca_V3.2$ display a reduction in their peak current evoked by a train of action potential waveform applied at frequencies of 50 Hz, while $Ca_V3.3$ displays an initial facilitation of peak current during successive action potential shaped stimulus trials due to a slower inactivation kinetic (Cazade, Bidaud, Lory, & Chemin, 2017; Chemin et al., 2002). In cells expressing the three Ca_V3 subtypes we found a decrease in current depression, which is consistent with a smaller contribution of $Ca_V3.3$ currents. Moreover, we found that D5R coexpression exacerbates the peak current depression, as expected if $Ca_V3.1$ is insensitive to its constitutive activity.

Finally, we show that D5R constitutive activity reduces the firing rate of action potentials through the reduction of Ca_V3 current *ex vivo*. Specifically, we observed a reduction in the rheobase value in the neurons from animals treated with CPZ while we found no differences in resting membrane potential or threshold membrane potential, indicating an increased neuronal excitability. Moreover, the specific Ca_V3 blocker TTA-P2 had the opposite effect in neurons from CPZ-treated animals. In this regard, the relationship between the density of Ca_V3 and the rheobase was already observed (Canto-Bustos et al., 2014; Huang et al., 2016; Jagodic et al., 2007; Tracy et al., 2018) and in particular Nigam et al. have shown that TTA-P2 was capable of increasing rheobase value in a model of temporal lobe epilepsy, where the Ca_V3 currents are upregulated (Nigam et al., 2019). On the other hand, since CA1 pyramidal neurons have a typical resting membrane potential of -70 mV it would be unlikely to have a contribution of Ca_V3 channels at these hyperpolarized values, considering that Ca_V3 reported window currents has a peak at -50 mV (Weiss &

Zamponi, 2019a).To complement these observations, we predicted *in silico* the impact of D5R constitutive activity on the firing rate by setting different levels of Ca_V3 current. In line with this, in pathophysiological states such as epilepsy, transcriptional upregulation of $Ca_V3.2$ associates with a change in the firing pattern (Becker et al., 2008) and a treatment with the selective Ca_V3 antagonist, Z944, diminishes the spinal excitability and the consequent pain hypersensitivity (Harding et al., 2021). Since several studies demonstrated that $Ca_V3.2$ expression is elevated in epileptic states (Powell, Cain, Snutch, & O'Brien, 2014), would be expected that CPZ, acting as an inverse agonist, increased the seizures episodes. In this regard, there are several published studies showing that antipsychotic drugs increase the risk for seizure induction (Gorska, Slupski, & Cubala, 2019). Conversely, others have shown that a loss-of-function mutation in $Ca_V3.2$ (by simulation of reduction in G_{max} using NEURON) associated with amyotrophic lateral sclerosis reduces the firing frequency of reticular thalamic neuron (Rzhepetskyy, Lazniewska, Blesneac, Pamphlett, & Weiss, 2016). Likewise, in patients with trigeminal neuralgia a $Ca_V3.2$ mutation that increases G_{max} has been recently associated with an increase in the firing frequency of trigeminal ganglion neurons (Gambeta, Gandini, Souza, & Zamponi, 2022). On the other hand, the acute application of the specific D1R/D5R agonist, SKF 38393, on CA1 pyramidal neurons partially restored electrophysiological alterations on potassium conductances and, consequently, on excitability and firing properties in a model of schizophrenia (Griego et al., 2022). Overall, our results showing a basal Ca_V3 current impairment by D1R/D5R constitutive activity support a chronic mechanism that could fine tune neuronal excitability.

5- Conclusions

Here we demonstrated a physiological and relevant mechanism of long-lasting modulation of Ca_V3 currents by D1R/D5R constitutive activity in hippocampal CA1 pyramidal neurons. In a heterologous expression system we found that only two out of three Ca_V3 subtypes are sensitive to D5R basal activity ($Ca_V3.2$ and $Ca_V3.3$). Moreover, we found an exacerbation on this effect under physiological significant voltage stimuli. Finally, we assayed the impact of this mechanism on firing frequency both *ex vivo* and *in silico*.

Bullet point summary

- **What its already known**
  - The dopamine receptor D5R displays high levels of constitutive activity *in vitro*.
  - Ca_V3 currents control neuronal firing patterns in physio- and pathophysiological states.

- **What this study adds**

- D1R/D5R constitutive activity reduces Ca_V3 currents and firing rate in hippocampal CA1 pyramidal neurons.
- $Ca_V3.2$ and $Ca_V3.3$ are specific targets of D5R constitutive activity.
-

- **Clinical significance**

- Chlorpromazine, a typical antipsychotic drug, reverses the D5R constitutive activity's effects.
- Controlling D5R constitutive activity could provide a tool to treat conditions such as epilepsy.

Author contributions

E.R.M. and J.R. designed the experiments; E.R.M. and C.I.M performed the patch clamp experiments; A.E.P. performed imaging experiments; S.S.R. provided excellent technical assistance. E.R.M. and C.I.M. analyzed the electrophysiological data; A.E.P. analyzed the imaging data; E.R.M and S.C.G performed computational neuronal simulation; E.R.M. and J.R. prepared the figures; E.R.M. and J.R. wrote the manuscript. All authors reviewed the manuscript.

Conflict of Interest

The authors declare that they have no conflict of interest.

Declaration of transparency: This declaration acknowledges that this paper adheres to the principles for transparent reporting and scientific rigour of preclinical research as stated in the BJP guidelines for Design and Analysis, and Animal Experimentation, and as recommended by funding agencies, publishers and others organizations with supporting research.

References

Agosti, F., Cordisco Gonzalez, S., Martinez Damonte, V., Tolosa, M. J., Di Siervi, N., Schioth, H. B., . . . Raingo, J. (2017). Melanocortin 4 receptor constitutive activity inhibits L-type voltage-gated calcium channels in neurons. *Neuroscience, 346*, 102-112. doi: 10.1016/j.neuroscience.2017.01.007

Aguado, C., Garcia-Madrona, S., Gil-Minguez, M., & Lujan, R. (2016). Ontogenic Changes and Differential Localization of T-type Ca(2+) Channel Subunits Cav3.1 and Cav3.2 in Mouse Hippocampus and Cerebellum. *Front Neuroanat, 10*, 83. doi: 10.3389/fnana.2016.00083

Al-Fulaij, M. A., Ren, Y., Beinborn, M., & Kopin, A. S. (2008). Pharmacological analysis of human D1 AND D2 dopamine receptor missense variants. *J Mol Neurosci, 34*(3), 211-223. doi: 10.1007/s12031-007-9030-x

Alexander, S. P., Christopoulos, A., Davenport, A. P., Kelly, E., Mathie, A., Peters, J. A., . . . Ye, R. D. (2021). THE CONCISE GUIDE TO PHARMACOLOGY 2021/22: G protein-coupled receptors. *Br J Pharmacol, 178 Suppl 1*, S27-S156. doi: 10.1111/bph.15538

Alexander, S. P., Mathie, A., Peters, J. A., Veale, E. L., Striessnig, J., Kelly, E., . . . Zhu, M. (2021). THE CONCISE GUIDE TO PHARMACOLOGY 2021/22: Ion channels. *Br J Pharmacol, 178 Suppl 1*, S157-S245. doi: 10.1111/bph.15539

Andrade, A., Hope, J., Allen, A., Yorgan, V., Lipscombe, D., & Pan, J. Q. (2016). A rare schizophrenia risk variant of CACNA1I disrupts CaV3.3 channel activity. *Sci Rep, 6*, 34233. doi: 10.1038/srep34233

Barrile, F., M'Kadmi, C., De Francesco, P. N., Cabral, A., Garcia Romero, G., Mustafa, E. R., . . . Perello, M. (2019). Development of a novel fluorescent ligand of growth hormone secretagogue receptor based on the N-Terminal Leap2 region. *Mol Cell Endocrinol, 498*, 110573. doi: 10.1016/j.mce.2019.110573

Becker, A. J., Pitsch, J., Sochivko, D., Opitz, T., Staniek, M., Chen, C. C., . . . Beck, H. (2008). Transcriptional upregulation of Cav3.2 mediates epileptogenesis in the pilocarpine model of epilepsy. *J Neurosci, 28*(49), 13341-13353. doi: 10.1523/JNEUROSCI.1421-08.2008

Bischofberger, J., Engel, D., Li, L., Geiger, J. R., & Jonas, P. (2006). Patch-clamp recording from mossy fiber terminals in hippocampal slices. *Nat Protoc, 1*(4), 2075-2081. doi: 10.1038/nprot.2006.312

Bozzi, Y., & Borrelli, E. (2013). The role of dopamine signaling in epileptogenesis. *Front Cell Neurosci, 7*, 157. doi: 10.3389/fncel.2013.00157

Cai, G., Gurdal, H., Smith, C., Wang, H. Y., & Friedman, E. (1999). Inverse agonist properties of dopaminergic antagonists at the D(1A) dopamine receptor: uncoupling of the D(1A) dopamine receptor from G(s) protein. *Mol Pharmacol, 56*(5), 989-996. doi: 10.1124/mol.56.5.989

Canto-Bustos, M., Loeza-Alcocer, E., Gonzalez-Ramirez, R., Gandini, M. A., Delgado-Lezama, R., & Felix, R. (2014). Functional expression of T-type Ca2+ channels in spinal motoneurons of the adult turtle. *PLoS One, 9*(9), e108187. doi: 10.1371/journal.pone.0108187

Castiglioni, A. J., Raingo, J., & Lipscombe, D. (2006). Alternative splicing in the C-terminus of CaV2.2 controls expression and gating of N-type calcium channels. *J Physiol, 576*(Pt 1), 119-134. doi: 10.1113/jphysiol.2006.115030

Cazade, M., Bidaud, I., Lory, P., & Chemin, J. (2017). Activity-dependent regulation of T-type calcium channels by submembrane calcium ions. *Elife, 6*. doi: 10.7554/eLife.22331

Conroy, J. L., Free, R. B., & Sibley, D. R. (2015). Identification of G protein-biased agonists that fail to recruit beta-arrestin or promote internalization of the D1 dopamine receptor. *ACS Chem Neurosci, 6*(4), 681-692. doi: 10.1021/acschemneuro.5b00020

Cordisco Gonzalez, S., Mustafa, E. R., Rodriguez, S. S., Perello, M., & Raingo, J. (2020). Dopamine Receptor Type 2 and Ghrelin Receptor Coexpression Alters CaV2.2 Modulation by G Protein Signaling Cascades. *ACS Chem Neurosci, 11*(1), 3-13. doi: 10.1021/acschemneuro.9b00426

Costa, T., & Cotecchia, S. (2005). Historical review: Negative efficacy and the constitutive activity of G-protein-coupled receptors. *Trends Pharmacol Sci, 26*(12), 618-624. doi: 10.1016/j.tips.2005.10.009

Chemin, J., Monteil, A., Perez-Reyes, E., Bourinet, E., Nargeot, J., & Lory, P. (2002). Specific contribution of human T-type calcium channel isotypes (alpha(1G), alpha(1H) and alpha(1I)) to neuronal excitability. *J Physiol, 540*(Pt 1), 3-14.

Chetrit, J., Taupignon, A., Froux, L., Morin, S., Bouali-Benazzouz, R., Naudet, F., . . . Benazzouz, A. (2013). Inhibiting subthalamic D5 receptor constitutive activity alleviates abnormal electrical activity and reverses motor impairment in a rat model of Parkinson's disease. *J Neurosci, 33*(37), 14840-14849. doi: 10.1523/JNEUROSCI.0453-13.2013

Choe, W., Messinger, R. B., Leach, E., Eckle, V. S., Obradovic, A., Salajegheh, R., . . . Todorovic, S. M. (2011). TTA-P2 is a potent and selective blocker of T-type calcium channels in rat sensory neurons and a novel antinociceptive agent. *Mol Pharmacol, 80*(5), 900-910. doi: 10.1124/mol.111.073205

Demchyshyn, L. L., McConkey, F., & Niznik, H. B. (2000). Dopamine D5 receptor agonist high affinity and constitutive activity profile conferred by carboxyl-terminal tail sequence. *J Biol Chem, 275*(31), 23446-23455. doi: 10.1074/jbc.M000157200

Dolphin, A. C. (2003). G protein modulation of voltage-gated calcium channels. *Pharmacol Rev, 55*(4), 607-627. doi: 10.1124/pr.55.4.3

Ertel, E. A., Campbell, K. P., Harpold, M. M., Hofmann, F., Mori, Y., Perez-Reyes, E., . . . Catterall, W. A. (2000). Nomenclature of voltage-gated calcium channels. *Neuron, 25*(3), 533-535.

Finlin, B. S., Crump, S. M., Satin, J., & Andres, D. A. (2003). Regulation of voltage-gated calcium channel activity by the Rem and Rad GTPases. *Proc Natl Acad Sci U S A, 100*(24), 14469-14474. doi: 10.1073/pnas.2437756100

Gainetdinov, R. R., Premont, R. T., Bohn, L. M., Lefkowitz, R. J., & Caron, M. G. (2004). Desensitization of G protein-coupled receptors and neuronal functions. *Annu Rev Neurosci, 27*, 107-144. doi: 10.1146/annurev.neuro.27.070203.144206

Gambeta, E., Gandini, M. A., Souza, I. A., & Zamponi, G. W. (2022). CaV3.2 calcium channels contribute to trigeminal neuralgia. *Pain*. doi: 10.1097/j.pain.0000000000002651

Gorska, N., Slupski, J., & Cubala, W. J. (2019). Antipsychotic drugs in epilepsy. *Neurol Neurochir Pol, 53*(6), 408-412. doi: 10.5603/PJNNS.a2019.0052

Griego, E., Hernandez-Frausto, M., Marquez, L. A., Lara-Valderrabano, L., Lopez Rubalcava, C., & Galvan, E. J. (2022). Activation of D1/D5 receptors ameliorates decreased intrinsic excitability of hippocampal neurons induced by neonatal blockade of N-methyl-d-aspartate receptors. *Br J Pharmacol, 179*(8), 1695-1715. doi: 10.1111/bph.15735

Harding, E. K., Dedek, A., Bonin, R. P., Salter, M. W., Snutch, T. P., & Hildebrand, M. E. (2021). The T-type calcium channel antagonist, Z944, reduces spinal excitability and pain hypersensitivity. *Br J Pharmacol, 178*(17), 3517-3532. doi: 10.1111/bph.15498

He, L., Yu, Z., Geng, Z., Huang, Z., Zhang, C., Dong, Y., . . . Zhao, Y. (2022). Structure, gating, and pharmacology of human CaV3.3 channel. *Nat Commun, 13*(1), 2084. doi: 10.1038/s41467-022-29728-0

Hildebrand, M. E., David, L. S., Hamid, J., Mulatz, K., Garcia, E., Zamponi, G. W., & Snutch, T. P. (2007). Selective inhibition of Cav3.3 T-type calcium channels by Galphaq/11-coupled muscarinic acetylcholine receptors. *J Biol Chem, 282*(29), 21043-21055. doi: 10.1074/jbc.M611809200

Hille, B. (1992). *Ionic channels of excitable membranes*.

Hines, M. L., & Carnevale, N. T. (1997). The NEURON simulation environment. *Neural Comput, 9*(6), 1179-1209.

Huang, D., Huang, S., Gao, H., Liu, Y., Qi, J., Chen, P., . . . Gamper, N. (2016). Redox-Dependent Modulation of T-Type Ca(2+) Channels in Sensory Neurons Contributes to Acute Anti-

Nociceptive Effect of Substance P. *Antioxid Redox Signal, 25*(5), 233-251. doi: 10.1089/ars.2015.6560

Jagodic, M. M., Pathirathna, S., Nelson, M. T., Mancuso, S., Joksovic, P. M., Rosenberg, E. R., . . . Todorovic, S. M. (2007). Cell-specific alterations of T-type calcium current in painful diabetic neuropathy enhance excitability of sensory neurons. *J Neurosci, 27*(12), 3305-3316. doi: 10.1523/JNEUROSCI.4866-06.2007

Karmazinova, M., Baumgart, J. P., Perez-Reyes, E., & Lacinova, L. (2011). The voltage dependence of gating currents of the neuronal CA(v)3.3 channel is determined by the gating brake in the I-II loop. *Pflugers Arch, 461*(4), 461-468. doi: 10.1007/s00424-011-0937-2

Karmazinova, M., Jaskova, K., Griac, P., Perez-Reyes, E., & Lacinova, L. (2015). Contrasting the roles of the I-II loop gating brake in CaV3.1 and CaV3.3 calcium channels. *Pflugers Arch, 467*(12), 2519-2527. doi: 10.1007/s00424-015-1728-y

Kisilevsky, A. E., Mulligan, S. J., Altier, C., Iftinca, M. C., Varela, D., Tai, C., . . . Zamponi, G. W. (2008). D1 receptors physically interact with N-type calcium channels to regulate channel distribution and dendritic calcium entry. *Neuron, 58*(4), 557-570. doi: 10.1016/j.neuron.2008.03.002

Klockner, U., Lee, J. H., Cribbs, L. L., Daud, A., Hescheler, J., Pereverzev, A., . . . Schneider, T. (1999). Comparison of the Ca2 + currents induced by expression of three cloned alpha1 subunits, alpha1G, alpha1H and alpha1I, of low-voltage-activated T-type Ca2 + channels. *Eur J Neurosci, 11*(12), 4171-4178. doi: 10.1046/j.1460-9568.1999.00849.x

Kortekaas, P., & Wadman, W. J. (1997). Development of HVA and LVA calcium currents in pyramidal CA1 neurons in the hippocampus of the rat. *Brain Res Dev Brain Res, 101*(1-2), 139-147. doi: 10.1016/s0165-3806(97)00059-x

Kraus, R. L., Li, Y., Gregan, Y., Gotter, A. L., Uebele, V. N., Fox, S. V., . . . Reger, T. S. (2010). In vitro characterization of T-type calcium channel antagonist TTA-A2 and in vivo effects on arousal in mice. *Journal of Pharmacology and Experimental Therapeutics, 335*(2), 409-417.

Lopez Soto, E. J., Agosti, F., Cabral, A., Mustafa, E. R., Damonte, V. M., Gandini, M. A., . . . Raingo, J. (2015). Constitutive and ghrelin-dependent GHSR1a activation impairs CaV2.1 and CaV2.2 currents in hypothalamic neurons. *J Gen Physiol, 146*(3), 205-219. doi: 10.1085/jgp.201511383

Martinez Damonte, V., Rodriguez, S. S., & Raingo, J. (2018). Growth hormone secretagogue receptor constitutive activity impairs voltage-gated calcium channel-dependent inhibitory neurotransmission in hippocampal neurons. *J Physiol, 596*(22), 5415-5428. doi: 10.1113/JP276256

McCarthy, C. I., Chou-Freed, C., Rodriguez, S. S., Yaneff, A., Davio, C., & Raingo, J. (2020). Constitutive activity of dopamine receptor type 1 (D1R) increases CaV2.2 currents in PFC neurons. *J Gen Physiol, 152*(5). doi: 10.1085/jgp.201912492

McKay, B. E., McRory, J. E., Molineux, M. L., Hamid, J., Snutch, T. P., Zamponi, G. W., & Turner, R. W. (2006). Ca(V)3 T-type calcium channel isoforms differentially distribute to somatic and dendritic compartments in rat central neurons. *Eur J Neurosci, 24*(9), 2581-2594. doi: 10.1111/j.1460-9568.2006.05136.x

Megat, S., Shiers, S., Moy, J. K., Barragan-Iglesias, P., Pradhan, G., Seal, R. P., . . . Price, T. J. (2018). A Critical Role for Dopamine D5 Receptors in Pain Chronicity in Male Mice. *J Neurosci, 38*(2), 379-397. doi: 10.1523/JNEUROSCI.2110-17.2017

Monteil, A., Chemin, J., Bourinet, E., Mennessier, G., Lory, P., & Nargeot, J. (2000). Molecular and functional properties of the human alpha(1G) subunit that forms T-type calcium channels. *J Biol Chem, 275*(9), 6090-6100. doi: 10.1074/jbc.275.9.6090

Monteil, A., Chemin, J., Leuranguer, V., Altier, C., Mennessier, G., Bourinet, E., . . . Nargeot, J. (2000). Specific properties of T-type calcium channels generated by the human alpha 1I subunit. *J Biol Chem, 275*(22), 16530-16535. doi: 10.1074/jbc.C000090200

Mustafa, E. R., Cordisco Gonzalez, S., Damian, M., Cantel, S., Denoyelle, S., Wagner, R., . . . Raingo, J. (2021). LEAP2 Impairs the Capability of the Growth Hormone Secretagogue Receptor to Regulate the Dopamine 2 Receptor Signaling. *Front Pharmacol, 12*, 712437. doi: 10.3389/fphar.2021.712437

Mustafa, E. R., Cordisco Gonzalez, S., & Raingo, J. (2020). Ghrelin Selectively Inhibits CaV3.3 Subtype of Low-Voltage-Gated Calcium Channels. *Mol Neurobiol, 57*(2), 722-735. doi: 10.1007/s12035-019-01738-y

Mustafa, E. R., Lopez Soto, E. J., Martinez Damonte, V., Rodriguez, S. S., Lipscombe, D., & Raingo, J. (2017). Constitutive activity of the Ghrelin receptor reduces surface expression of voltage-gated Ca(2+) channels in a CaVbeta-dependent manner. *J Cell Sci, 130*(22), 3907-3917. doi: 10.1242/jcs.207886

Nichols, D. E. (2010). Dopamine receptor subtype-selective drugs: D1-like receptors *The Dopamine Receptors* (pp. 75-99): Springer.

Nigam, A., Hargus, N. J., Barker, B. S., Ottolini, M., Hounshell, J. A., Bertram, E. H., 3rd, . . . Patel, M. K. (2019). Inhibition of T-Type calcium channels in mEC layer II stellate neurons reduces neuronal hyperexcitability associated with epilepsy. *Epilepsy Res, 154*, 132-138. doi: 10.1016/j.eplepsyres.2019.05.006

Pantel, J., Legendre, M., Cabrol, S., Hilal, L., Hajaji, Y., Morisset, S., . . . Amselem, S. (2006). Loss of constitutive activity of the growth hormone secretagogue receptor in familial short stature. *J Clin Invest, 116*(3), 760-768. doi: 10.1172/JCI25303

Paz, R. M., Stahl, A. M., Rela, L., Murer, M. G., & Tubert, C. (2022). D1/D5 Inverse Agonists Restore Striatal Cholinergic Interneuron Physiology in Dyskinetic Mice. *Mov Disord*. doi: 10.1002/mds.29055

Percie du Sert, N., Hurst, V., Ahluwalia, A., Alam, S., Avey, M. T., Baker, M., . . . Wurbel, H. (2020). The ARRIVE guidelines 2.0: updated guidelines for reporting animal research. *BMJ Open Sci, 4*(1), e100115. doi: 10.1136/bmjos-2020-100115

Perez-Reyes, E. (2003). Molecular physiology of low-voltage-activated t-type calcium channels. *Physiol Rev, 83*(1), 117-161. doi: 10.1152/physrev.00018.2002

Powell, K. L., Cain, S. M., Snutch, T. P., & O'Brien, T. J. (2014). Low threshold T-type calcium channels as targets for novel epilepsy treatments. *Br J Clin Pharmacol, 77*(5), 729-739. doi: 10.1111/bcp.12205

Proft, J., & Weiss, N. (2015). G protein regulation of neuronal calcium channels: back to the future. *Mol Pharmacol, 87*(6), 890-906. doi: 10.1124/mol.114.096008

Rangel, A., Sanchez-Armass, S., & Meza, U. (2010). Protein kinase C-mediated inhibition of recombinant T-type Cav3.2 channels by neurokinin 1 receptors. *Mol Pharmacol, 77*(2), 202-210. doi: 10.1124/mol.109.058727

Rojo, D., McCarthy, C., Raingo, J., & Rubinstein, M. (2020). Mouse models for V103I and I251L gain of function variants of the human MC4R display decreased adiposity but are not protected against a hypercaloric diet. *Mol Metab, 42*, 101077. doi: 10.1016/j.molmet.2020.101077

Rzhepetskyy, Y., Lazniewska, J., Blesneac, I., Pamphlett, R., & Weiss, N. (2016). CACNA1H missense mutations associated with amyotrophic lateral sclerosis alter Cav3.2 T-type calcium channel activity and reticular thalamic neuron firing. *Channels (Austin), 10*(6), 466-477. doi: 10.1080/19336950.2016.1204497

Sahu, A., Tyeryar, K. R., Vongtau, H. O., Sibley, D. R., & Undieh, A. S. (2009). D5 dopamine receptors are required for dopaminergic activation of phospholipase C. *Mol Pharmacol, 75*(3), 447-453. doi: 10.1124/mol.108.053017

Sanabria, E. R., Su, H., & Yaari, Y. (2001). Initiation of network bursts by Ca2+-dependent intrinsic bursting in the rat pilocarpine model of temporal lobe epilepsy. *J Physiol, 532*(Pt 1), 205-216. doi: 10.1111/j.1469-7793.2001.0205g.x

Sarinana, J., Kitamura, T., Kunzler, P., Sultzman, L., & Tonegawa, S. (2014). Differential roles of the dopamine 1-class receptors, D1R and D5R, in hippocampal dependent memory. *Proc Natl Acad Sci U S A, 111*(22), 8245-8250. doi: 10.1073/pnas.1407395111

Sasamori, H., Asakura, T., Sugiura, C., Bouchekioua, Y., Nishitani, N., Sato, M., . . . Yoshioka, M. (2022). Behavioral characteristics of dopamine D5 receptor knockout mice. *Sci Rep, 12*(1), 6014. doi: 10.1038/s41598-022-10013-5

Schindelin, J., Arganda-Carreras, I., Frise, E., Kaynig, V., Longair, M., Pietzsch, T., . . . Cardona, A. (2012). Fiji: an open-source platform for biological-image analysis. *Nat Methods, 9*(7), 676-682. doi: 10.1038/nmeth.2019

Snutch, T. P., & Zamponi, G. W. (2018). Recent advances in the development of T-type calcium channel blockers for pain intervention. *Br J Pharmacol, 175*(12), 2375-2383. doi: 10.1111/bph.13906

Stringer, R. N., Jurkovicova-Tarabova, B., Huang, S., Haji-Ghassemi, O., Idoux, R., Liashenko, A., . . . Weiss, N. (2020). A rare CACNA1H variant associated with amyotrophic lateral sclerosis causes complete loss of Cav3.2 T-type channel activity. *Mol Brain, 13*(1), 33. doi: 10.1186/s13041-020-00577-6

Tiberi, M., & Caron, M. G. (1994). High agonist-independent activity is a distinguishing feature of the dopamine D1B receptor subtype. *J Biol Chem, 269*(45), 27925-27931.

Torz, L. J., Osborne-Lawrence, S., Rodriguez, J., He, Z., Cornejo, M. P., Mustafa, E. R., . . . Zigman, J. M. (2020). Metabolic insights from a GHSR-A203E mutant mouse model. *Mol Metab, 39*, 101004. doi: 10.1016/j.molmet.2020.101004

Tracy, M. E., Tesic, V., Stamenic, T. T., Joksimovic, S. M., Busquet, N., Jevtovic-Todorovic, V., & Todorovic, S. M. (2018). CaV3.1 isoform of T-type calcium channels supports excitability of rat and mouse ventral tegmental area neurons. *Neuropharmacology, 135*, 343-354. doi: 10.1016/j.neuropharm.2018.03.028

Tsien, R. (1983). Calcium channels in excitable cell membranes. *Annu Rev Physiol, 45*(1), 341-358.

Uebachs, M., Opitz, T., Royeck, M., Dickhof, G., Horstmann, M. T., Isom, L. L., & Beck, H. (2010). Efficacy loss of the anticonvulsant carbamazepine in mice lacking sodium channel beta subunits via paradoxical effects on persistent sodium currents. *J Neurosci, 30*(25), 8489-8501. doi: 10.1523/JNEUROSCI.1534-10.2010

Weiss, N., & Zamponi, G. W. (2019a). T-type calcium channels: From molecule to therapeutic opportunities. *Int J Biochem Cell Biol, 108*, 34-39. doi: 10.1016/j.biocel.2019.01.008

Weiss, N., & Zamponi, G. W. (2019b). T-Type Channel Druggability at a Crossroads. *ACS Chem Neurosci, 10*(3), 1124-1126. doi: 10.1021/acschemneuro.9b00031

Wolfe, J. T., Wang, H., Howard, J., Garrison, J. C., & Barrett, P. Q. (2003). T-type calcium channel regulation by specific G-protein betagamma subunits. *Nature, 424*(6945), 209-213. doi: 10.1038/nature01772

Wootten, D., Christopoulos, A., Marti-Solano, M., Babu, M. M., & Sexton, P. M. (2018). Mechanisms of signalling and biased agonism in G protein-coupled receptors. *Nat Rev Mol Cell Biol, 19*(10), 638-653. doi: 10.1038/s41580-018-0049-3

Xiong, G., Metheny, H., Johnson, B. N., & Cohen, A. S. (2017). A Comparison of Different Slicing Planes in Preservation of Major Hippocampal Pathway Fibers in the Mouse. *Front Neuroanat, 11*, 107. doi: 10.3389/fnana.2017.00107

You, H., Altier, C., & Zamponi, G. W. (2010). CCR2 receptor ligands inhibit Cav3.2 T-type calcium channels. *Mol Pharmacol, 77*(2), 211-217. doi: 10.1124/mol.109.059022

Yunker, A. M., Sharp, A. H., Sundarraj, S., Ranganathan, V., Copeland, T. D., & McEnery, M. W. (2003). Immunological characterization of T-type voltage-dependent calcium channel CaV3.1 (alpha 1G) and CaV3.3 (alpha 1I) isoforms reveal differences in their localization, expression, and neural development. *Neuroscience, 117*(2), 321-335.

Zhang, B., Albaker, A., Plouffe, B., Lefebvre, C., & Tiberi, M. (2014). Constitutive activities and inverse agonism in dopamine receptors. *Adv Pharmacol, 70*, 175-214. doi: 10.1016/B978-0-12-417197-8.00007-9

Zhang, B., Yang, X., & Tiberi, M. (2015). Functional importance of two conserved residues in intracellular loop 1 and transmembrane region 2 of Family A GPCRs: insights from ligand binding and signal transduction responses of D1 and D5 dopaminergic receptor mutants. *Cell Signal, 27*(10), 2014-2025. doi: 10.1016/j.cellsig.2015.07.006

Zhang, Y., Jiang, X., Snutch, T. P., & Tao, J. (2013). Modulation of low-voltage-activated T-type Ca(2)(+) channels. *Biochim Biophys Acta, 1828*(7), 1550-1559. doi: 10.1016/j.bbamem.2012.08.032

Zhao, Y., Huang, G., Wu, Q., Wu, K., Li, R., Lei, J., . . . Yan, N. (2019). Cryo-EM structures of apo and antagonist-bound human Cav3.1. *Nature, 576*(7787), 492-497. doi: 10.1038/s41586-019-1801-3
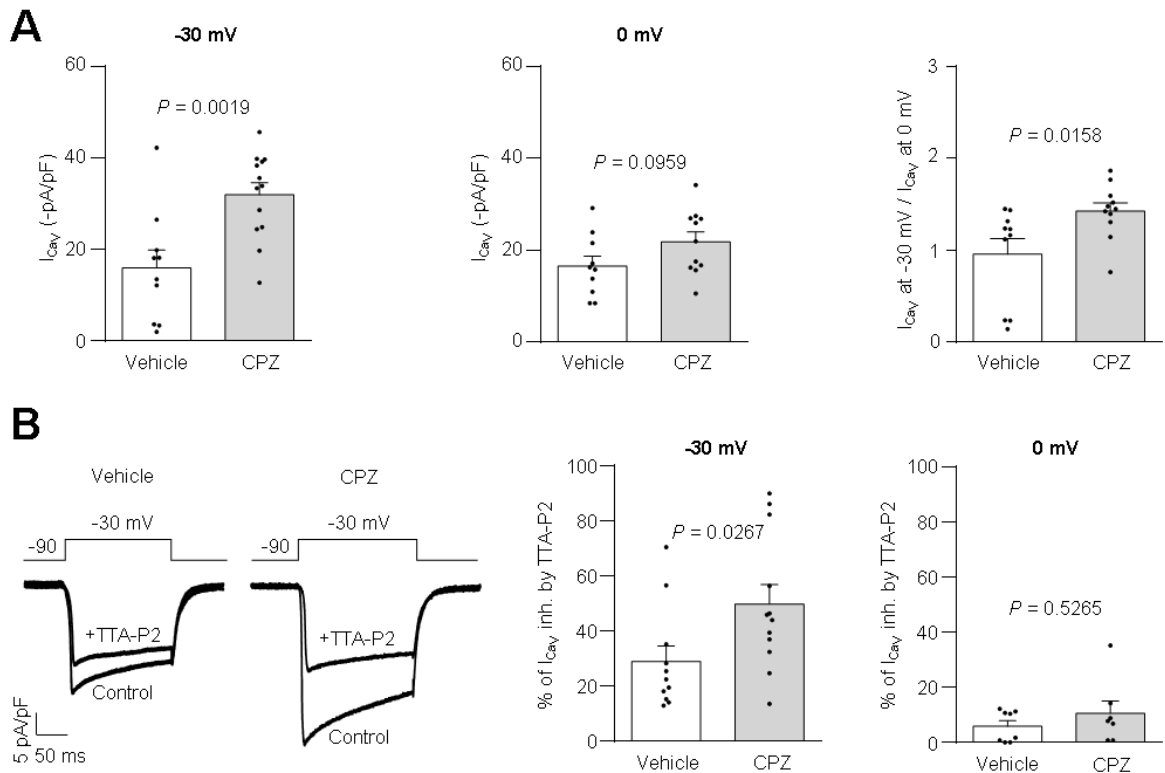
Figure 1

Figure 1. (A) Bars (left) represent the averaged calcium current (I$_{CaV}$) registered with a pulse from -90 mV to -30 mV in CA1 pyramidal neurons of mice hippocampus treated i.p. with vehicle (N = 10, 4 animals) or chlorpromazine (CPZ; N = 13, 3 animals). Bars (middle) represent the averaged I$_{CaV}$ registered with a pulse from -90 mV to 0 mV in CA1 pyramidal neurons of mice hippocampus treated i.p. with vehicle (N = 10, 4 animals) or chlorpromazine (CPZ; N = 11, 3 animals). Statistical significance was evaluated by One-Sample Student's t test. Bars (right) represent the averaged ratio I$_{CaV}$ at -30 mV / I$_{CaV}$ at 0 mV in CA1 pyramidal neurons of mice hippocampus treated i.p. with vehicle (N = 10, 4 animals) or chlorpromazine (CPZ; N = 11, 3 animals). Statistical significance was evaluated by Mann-Whitney test. **(B)** Representative traces (right), averaged percentage of I$_{CaV}$ inhibition by TTA-P2 in CA1 pyramidal neurons of mice hippocampus treated i.p. with vehicle (N = 11, 4 animals) or chlorpromazine (CPZ; N = 12, 3 animals) at -30 mV (middle) and averaged percentage of I$_{CaV}$ inhibition by TTA-P2 in CA1 pyramidal neurons of mice hippocampus treated i.p. with vehicle (N = 8, 4 animals) or chlorpromazine (CPZ; N = 7, 3 animals) at 0 mV (right). CPZ; 1 mg/kg. TTA-P2; 1 μM. Statistical significance was evaluated by Mann-Whitney test.
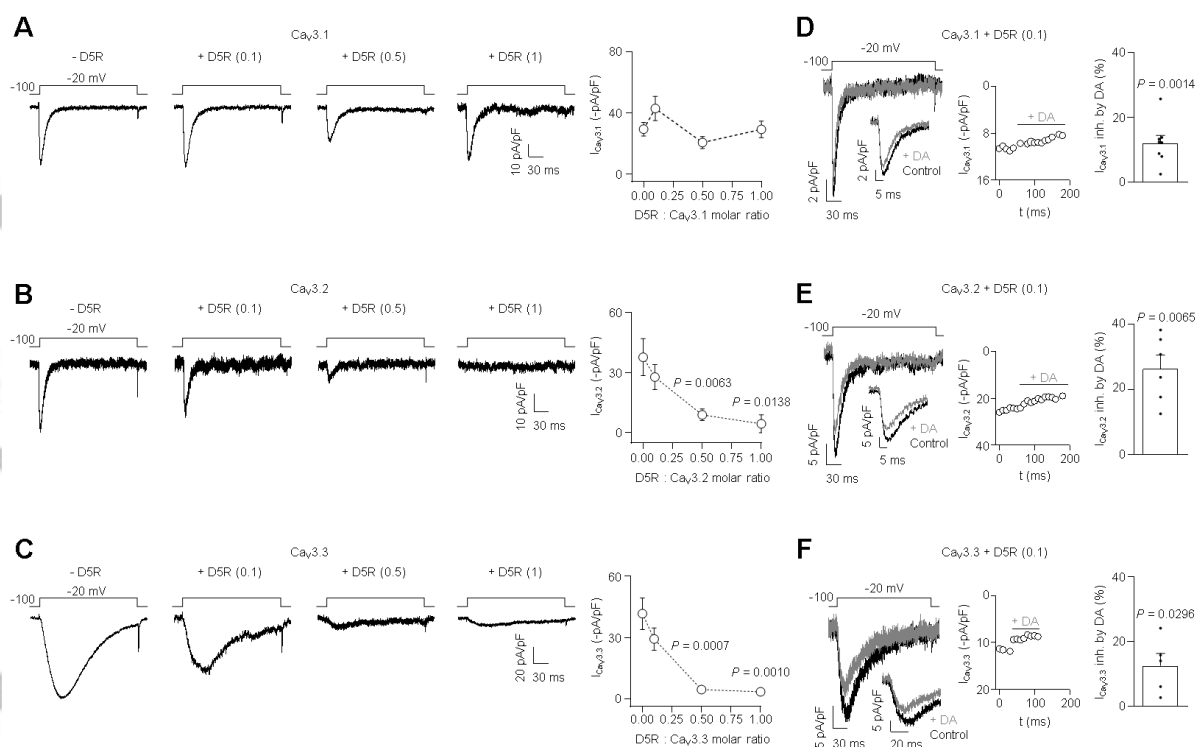
Figure 2

Figure 2. (A) Representative traces (left) of Ca$_V$3.1 current (I$_{CaV3.1}$) from HEK293T cells cotransfected with Ca$_V$3.1 and pcDNA3.1 (- D5R, N = 20) or with D5R in 0.1 (+ D5R (0.1), N = 11), 0.5 (+ D5R (0.5), N = 11) or 1 (+ D5R (1), N = 16) D5R: Ca$_V$3.1 molar ratio. Dots (right) represent averaged I$_{CaV3.1}$ for each condition. **(B)** Representative traces (left) of Ca$_V$3.2 current (I$_{CaV3.2}$) from HEK293T cells cotransfected with Ca$_V$3.2 and pcDNA3.1 (- D5R, N = 7) or with D5R in 0.1 (+ D5R (0.1), N = 7), 0.5 (+ D5R (0.5), N = 6) or 1 (+ D5R (1), N = 5) D5R: Ca$_V$3.2 molar ratio. Dots (right) represent averaged I$_{CaV3.2}$ for each condition **(C)** Representative traces (left) of Ca$_V$3.3 current (I$_{CaV3.3}$) from HEK293T cells cotransfected with Ca$_V$3.3 and pcDNA3.1 (- D5R, N = 12) or with D5R in 0.1 (+ D5R (0.1), N = 10), 0.5 (+ D5R (0.5), N = 7) or 1 (+ D5R (1), N = 6) D5R: Ca$_V$3.3 molar ratio. Dots (right) represent averaged I$_{CaV3.3}$ for each condition. **(D)** Representative whole and inset traces (left) and time course (middle) of I$_{CaV3.1}$ from HEK293T cells cotransfected with Cav3.1 and D5R in 0.1 D5R: Cav3.1 molar ratio in control condition and dopamine application (+ DA, N = 8). Bar (right) represents averaged I$_{CaV3.1}$ inhibition by DA. . **(E)** Representative whole and inset traces (left) and time course (middle) of I$_{CaV3.2}$ from HEK293T cells cotransfected with Cav3.2 and D5R in 0.1 D5R: Cav3.2 molar ratio in control condition and DA application (+ DA, N = 9). Bar (right) represents averaged I$_{CaV3.2}$ inhibition by DA. **(F)** Representative traces (left) and time course (middle) of I$_{CaV3.3}$ from HEK293T cells cotransfected with Cav3.3 and D5R in 0.1 D5R: Cav3.3 molar ratio in control condition and DA application (+ DA, N = 5). Bar (right) represents averaged I$_{CaV3.3}$ inhibition by DA. DA; 10 µM. Statistical significance was

evaluated by Kruskal-Wallis and Dunn's post-test versus – D5R (panels A, B and C). Statistical significance was evaluated by One-Sample Student's t test versus 0 (panels D, E and F).
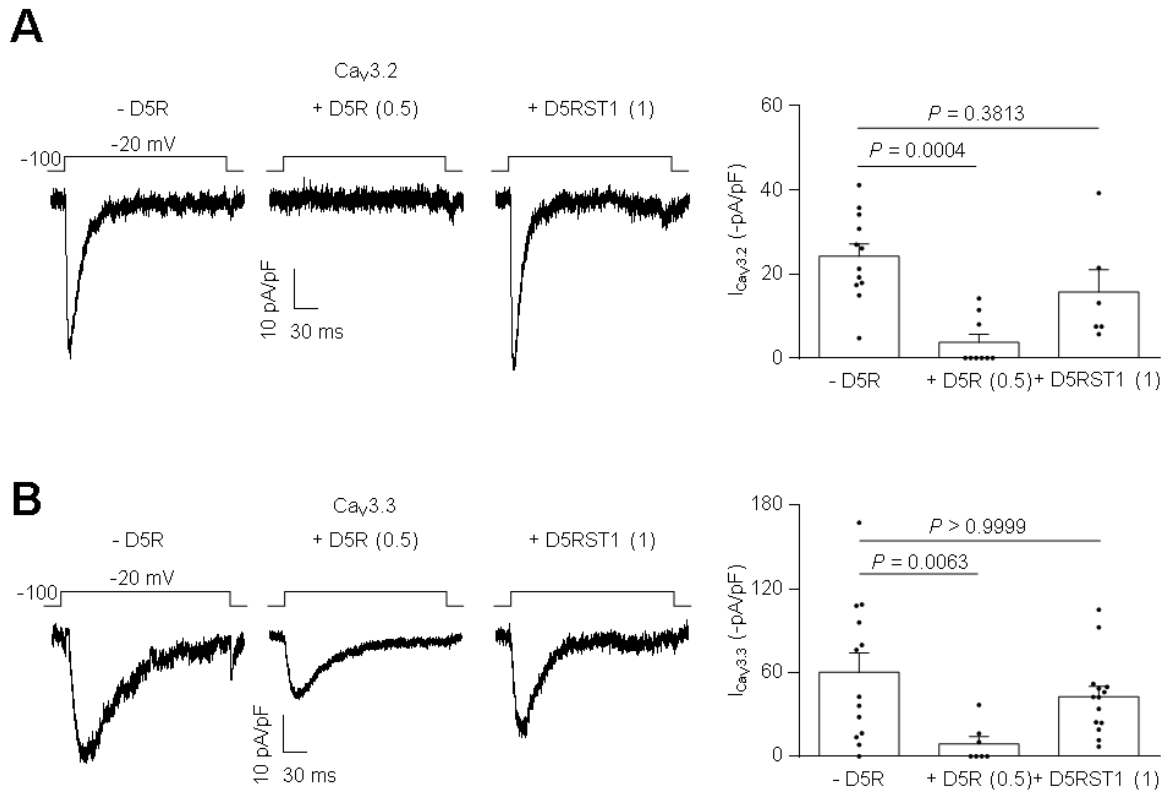
A

Ca$_V$3.2

- D5R   + D5R (0.5)   + D5RST1 (1)

B

Ca$_V$3.3

- D5R   + D5R (0.5)   + D5RST1 (1)

Figure 3

Figure 3. *(A)* Representative traces (left) of Ca$_V$3.2 current (I$_{CaV3.2}$) from HEK293T cells cotransfected with Ca$_V$3.2 and pcDNA3.1 (- D5R, N = 12) or with D5R in 0.5 (+ D5R (0.5), N = 9) or with D5RST1 (+ D5RST1 (1), N = 6) in 1 D5R: Ca$_V$3.2 molar ratio. Bars (right) represent averaged I$_{CaV3.2}$ for each condition. *(B)* Representative traces (left) of Ca$_V$3.3 current (I$_{CaV3.3}$) from HEK293T cells cotransfected with Ca$_V$3.3 and pcDNA3.1 (- D5R, N = 13) or with D5R in 0.5 (+ D5R (0.5), N = 7) or with D5RST1 (+ D5RST1 (1), N = 14) in 1 D1R:Ca$_V$3.3 molar ratio. Bars (right) represent averaged I$_{CaV3.3}$ for each condition. Statistical significance was evaluated by Kruskal-Wallis and Dunn's post-test versus – D5R for panels A and B.
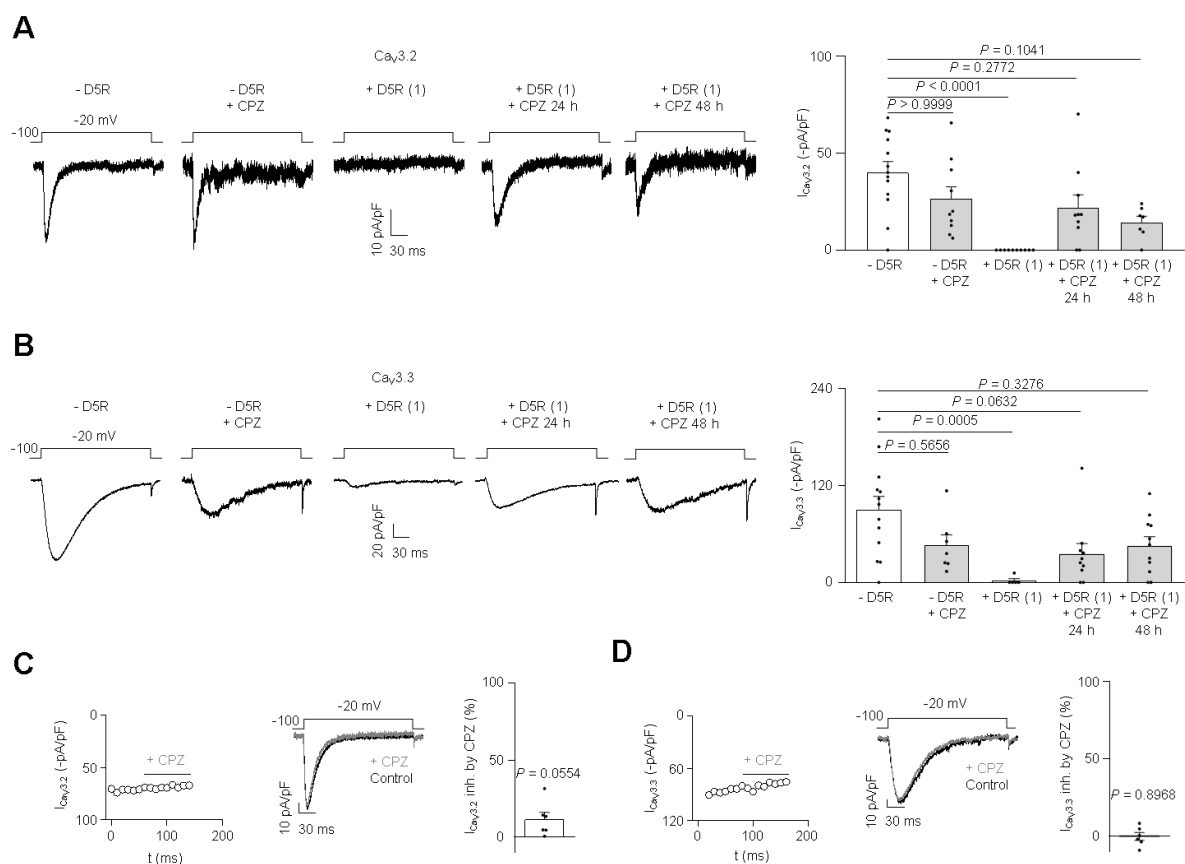
Figure 4

Figure 4. (A) Representative traces (left) of Ca$_V$3.2 current (I$_{CaV3.2}$) from HEK293T cells cotransfected with Ca$_V$3.2 and pcDNA3.1 preincubated (- D5R + CPZ, N = 10) or not with chlorpromazine (CPZ) (- D5R, N = 13) or with D5R in 1 D5R: Ca$_V$3.2 molar ratio preincubated for 24 h (+ D5R (1) + CPZ 24 h, N = 10) or 48 h (+ D5R (1) + CPZ 48 h, N = 7) or not with (1 μM) CPZ (+ D5R (1), N = 10). Bars (right) represent averaged I$_{CaV3.2}$ for each condition **(B)** Representative traces (left) of Ca$_V$3.3 current (I$_{CaV3.3}$) from HEK293T cells cotransfected with Ca$_V$3.3 and pcDNA3.1 preincubated (- D5R + CPZ, N = 7) or not with CPZ (- D5R, N = 13) or with D5R in 1 D5R: Ca$_V$3.3 molar ratio preincubated for 24 h (+ D5R (1) + CPZ 24 h, N = 9) or 48 h (+ D5R (1) + CPZ 48 h, N = 11) or not with CPZ (+ D5R (1), N = 6). Bars (right) represent averaged I$_{CaV3.3}$ for each condition. **(C)** Representative traces and time course (left) of I$_{CaV3.2}$ from HEK293T cells transfected with Cav3.2 in control condition and CPZ application (+ CPZ, N = 6). Bar (right) represents averaged I$_{CaV3.2}$ inhibition by CPZ. **(D)** Representative traces and time course (left) of I$_{CaV3.3}$ from HEK293T cells transfected with Ca$_V$3.3 in control condition and CPZ application (+ CPZ, N = 6). Bar (right) represents averaged I$_{CaV3.3}$ inhibition by CPZ. CPZ; 1 μM. Statistical significance was evaluated by Kruskal-Wallis and Dunn's post-test versus – D5R (panels A and B). Statistical significance was evaluated by One-Sample Student's t test versus 0 (panels C and D).
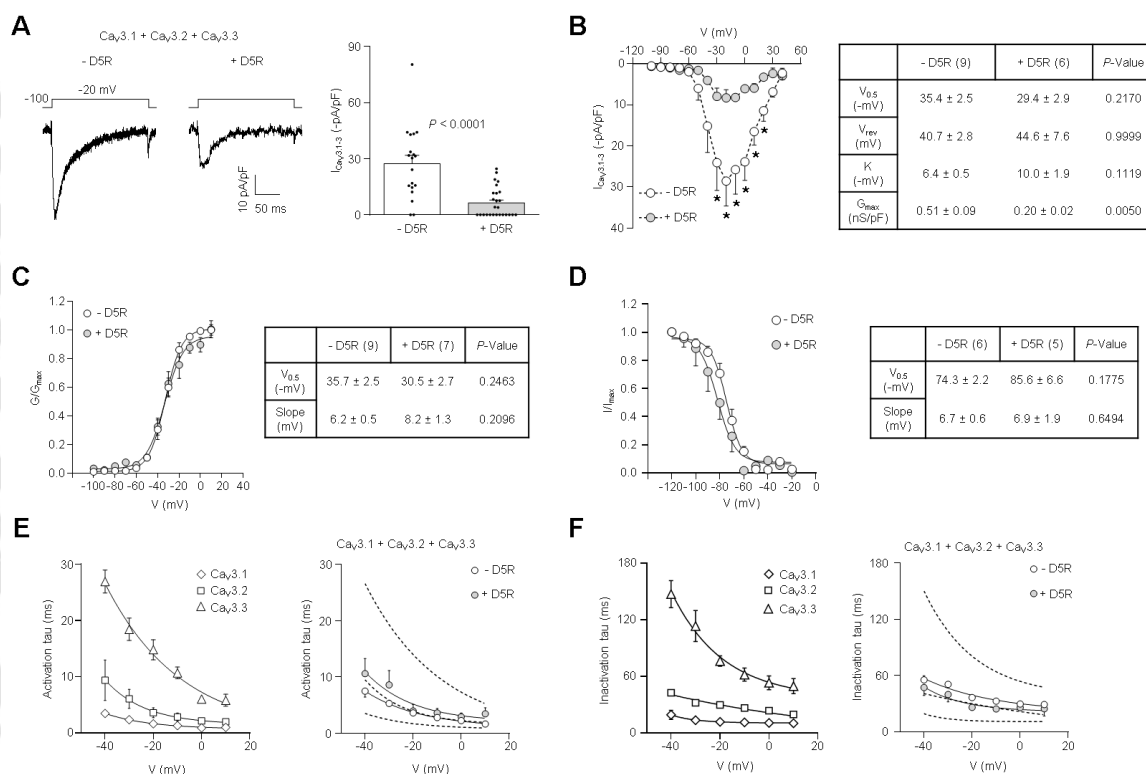
Figure 5

Figure 5. **(A)** Representative traces (left) of calcium current ($I_{CaV3.1-3}$) from HEK293T cells cotransfected with $Ca_V3.1$, $Ca_V3.2$, $Ca_V3.3$ with pcDNA3.1 (- D5R, N = 19) or with D5R (+ D5R, N = 26) in 1:1:1:3 $Ca_V3.1$: $Ca_V3.2$: $Ca_V3.3$: D5R molar ratio. Bars (right) represent averaged $I_{CaV3.1-3}$ for both conditions. Statistical significance was evaluated by Mann-Whitney test. **(B)** Averaged calcium current peak–voltage (I–V) relationship (left) from HEK293T cells cotransfected with $Ca_V3.1$, $Ca_V3.2$, $Ca_V3.3$ and pcDNA3.1 (- D5R, N = 9) or with D5R (+ D5R, N = 6). Stars represent statistical differences with $P < 0.05$. Unpaired sample Student's t test. Table (right) shows the average $V_{0.5}$, V_{rev}, K, and G_{max} values obtained in − D5R and + D5R conditions. The P values were obtained with unpaired sample Student's t test. **(C)** Averaged G/G_{max} versus voltage relationship (left). Line represents the fitted Boltzmann function in − D5R (N = 9) and + D5R (N = 7) conditions. Extra sum-of-square F test. F = 1.144 (DFn = 4, DFd = 176), $P = 0.2223$. Table (right) shows the $V_{0.5}$ and slope values obtained in − D5R and + D5R conditions. The P values were obtained with unpaired sample Student's t test. **(D)** Voltage dependence of inactivation and Boltzmann fit (left) in − D5R (N = 6) and + D5R (N = 5) conditions. Extra sum-of-square F test. F = 1.170 (DFn = 4, DFd = 113), $P = 0.3279$. Table (right) show the average $V_{0.5}$ and slope values obtained in − D5R and + D5R conditions. The P values were obtained with unpaired sample Student's t test. **(E)** Average activation tau values are plotted as a function of test potentials (left) for individual experiments expressing $Ca_V3.1$ (N = 6), $Ca_V3.2$ (N = 5) or $Ca_V3.3$ (N = 7) on HEK293T cells. Lines represent fitted single exponential function for each experiment.

Average activation tau values are plotted as a function of test potentials (right). Lines represent the fitted single exponential function in – D5R (N = 17) and + D5R (N = 9) conditions. Dash lines represent fitted single function for Ca$_V$3.1, Ca$_V$3.2 or Ca$_V$3.3 obtained in individual experiments. Unpaired sample Student's t test for each voltage. *(F)* Average inactivation tau values are plotted as a function of test potentials (left) for individual experiments expressing Ca$_V$3.1 (N = 6), Ca$_V$3.2 (N = 5) or Ca$_V$3.3 (N = 7) on HEK293T cells. Dash lines represent fitted single function for each experiment. Average inactivation tau values are plotted as a function of test potentials (right). Lines represent the fitted single exponential function in – D5R (N = 17) and + D5R (N = 9) conditions. Dash lines represent fitted single function for Ca$_V$3.1, Ca$_V$3.2 or Ca$_V$3.3 obtained in individual experiments. Unpaired sample Student's t test for each voltage.
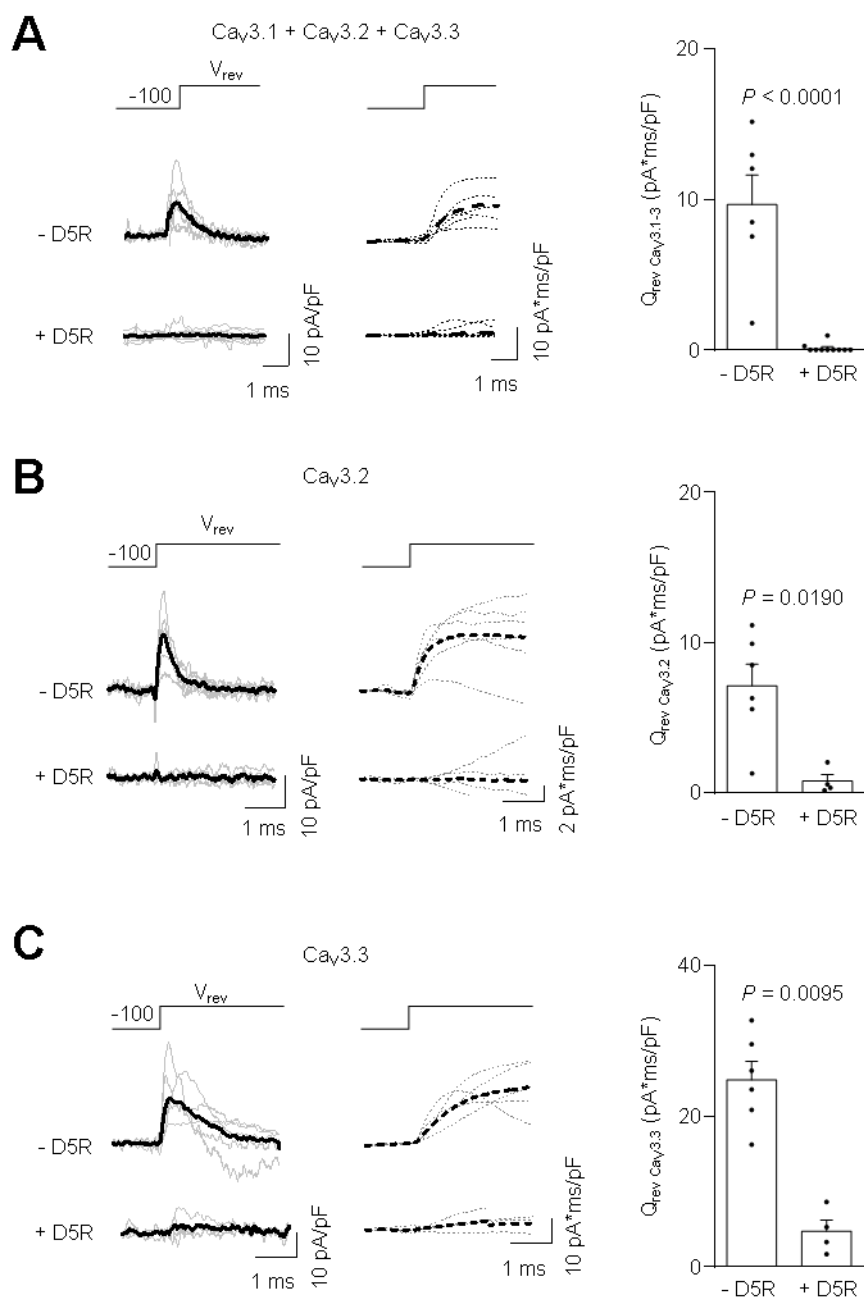
Figure 6

Figure 6. *(A)* Individual (gray) and averaged (black) traces of ON gating Ca_V3 currents at the reversal potential (left) and averaged Q_{rev} (right) from HEK293T cells cotransfected with $Ca_V3.1$, $Ca_V3.2$, $Ca_V3.3$ with pcDNA3.1 (- D5R, N = 6) or with D5R (+ D5R, N = 10) in 1:1:1:3 $Ca_V3.1$: $Ca_V3.2$: $Ca_V3.3$: D5R molar ratio. Individual (gray dash line) and averaged (black dash line) of integrated Ca_V3 ON gating currents showed at the left for both experimental conditions. **(B)** Individual (gray) and averaged (black) traces of $Ca_V3.2$ ON gating currents at the reversal potential and averaged Q_{rev} from HEK293T cells cotransfected with $Ca_V3.2$ and pcDNA3.1 (- D5R, N = 6) or D5R (+ D5R, N = 4) in 1:1

Ca$_V$3.2: D5R molar ratio. Individual (gray dash line) and averaged (black dash line) of integrated Ca$_V$3.2 ON gating currents showed at the left for both experimental conditions. **(C)** Individual (gray) and averaged (black) traces of Ca$_V$3.3 ON gating currents at the reversal potential and averaged Q$_{rev}$ from HEK293T cells cotransfected with Ca$_V$3.3 and pcDNA3.1 (-D5R, N = 6) or D5R (+ D5R, N = 4) in 1:1 Ca$_V$3.3: D5R molar ratio. Individual (gray dash line) and averaged (black dash line) of integrated Ca$_V$3.3 ON gating currents showed at the left for both experimental conditions. Reversal potential (V$_{rev}$, ~ 40 mV) was estimated individually for each cell. Statistical significance was evaluated by Mann-Whitney test for panels A, B and C.
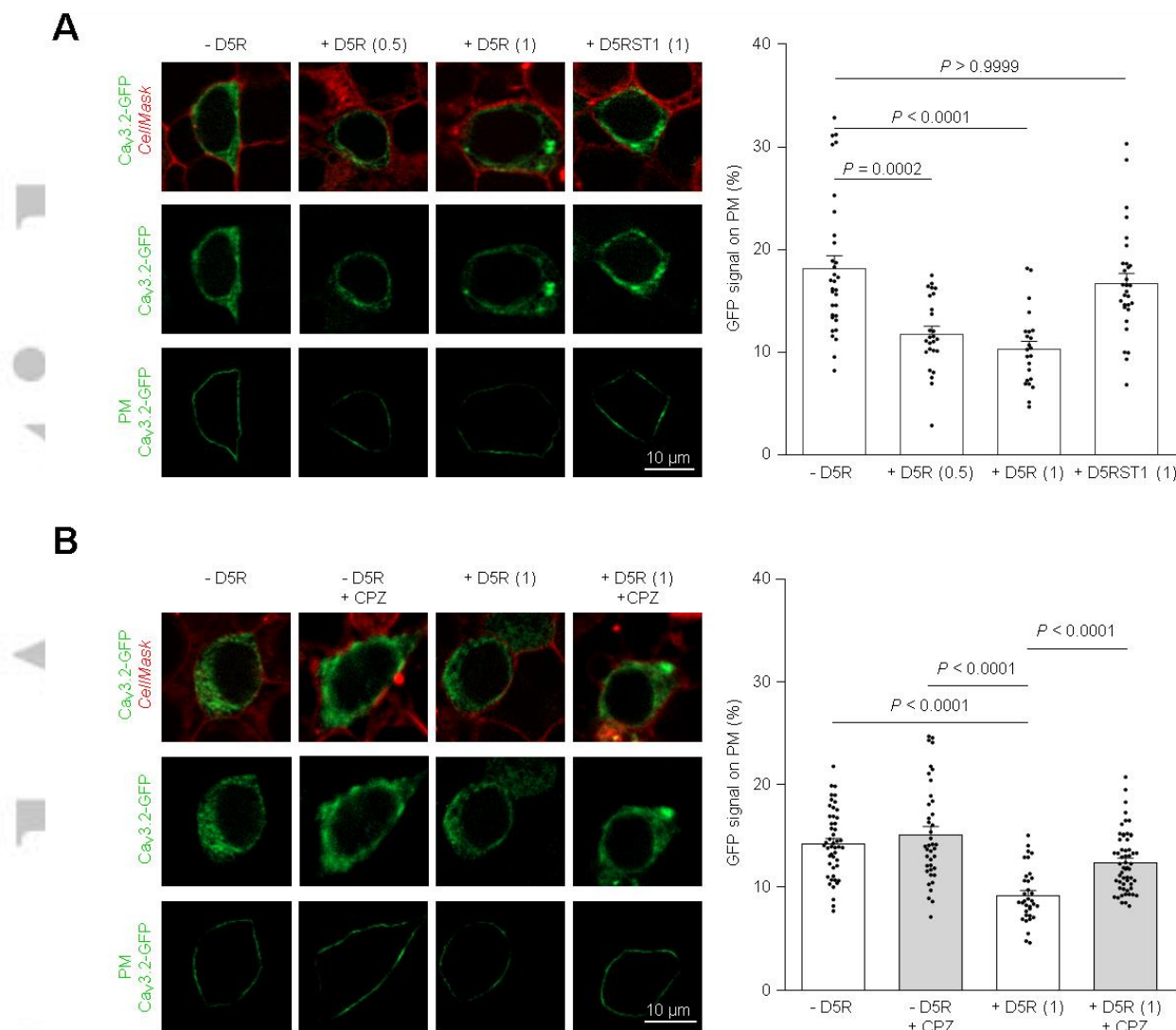
Figure 7

Figure 7. **(A)** Representative photomicrographs (left) and average percent of GFP plasma membrane (PM) signal (right) of HEK293T cells cotransfected with $Ca_V3.2$-GFP alone (-D5R, N = 32) or plus D5R in 1 D5R: $Ca_V3.2$ molar ratio (+D5R (1), N = 27), D5R in 0.5 D5R: $Ca_V3.2$ molar ratio (+D5R (0.5), N = 23) or D5RST1 in 1 D5RST1: $Ca_V3.2$ molar ratio (+D5RST1 (1), N = 30). . Statistical significance was evaluated by Kruskal-Wallis and Dunn's post-test versus – D5R. **(B)** Representative photomicrographs (left) and average percent of GFP PM signal (right) of HEK293T cells cotransfected with $Ca_V3.2$-GFP preincubated (-D5R + CPZ, N= 48) or not with CPZ (- D5R, N = 40) or with D5R preincubated (+D5R (1) + CPZ, N= 57) or not with CPZ (+ D5R, N=34) in 1 D5R: $Ca_V3.2$ molar ratio. Statistical significance was evaluated by Kruskal-Wallis and Dunn's post-test versus + D5R. Magnification: 40X. Green and red signals correspond to the GFP tag on $Ca_V3.2$ and the CellMask membrane marker respectively. In the photomicrographs panel the first row shows the merged signals

of total GFP and CellMask, the second row shows the signal of total GFP, and the third row shows the signal of GFP located at the PM.

Figure 8

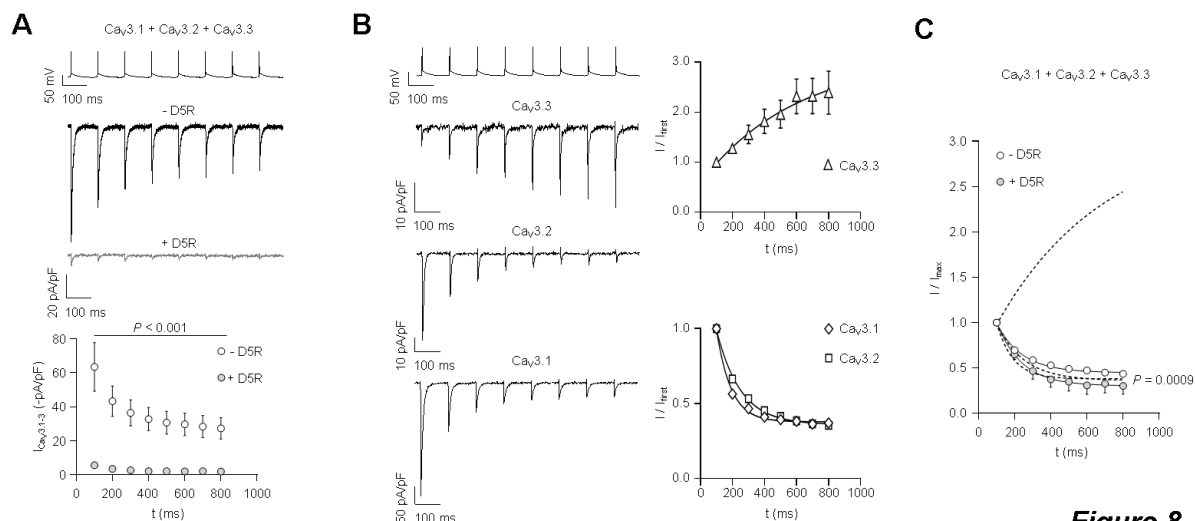**Figure 8. (A)** Representative traces (top) of calcium current ($I_{CaV3.1-3}$) from HEK293T cells cotransfected with $Ca_V3.1$, $Ca_V3.2$, $Ca_V3.3$ with pcDNA3.1 (-D5R, N = 8) or with D5R (+D5R, N = 18) in 1:1:1:3 $Ca_V3.1$:$Ca_V3.2$:$Ca_V3.3$:D5R molar ratio activated by a train of action potentials recorded from a CA1 neuron as command voltages. Dots (bottom) represent averaged $I_{CaV3.1-3}$ for both conditions. Statistical significance was evaluated by Mann-Whitney test for each time. **(B)** Representative traces (left) of calcium current from HEK293T cells cotransfected with $Ca_V3.3$ (N = 6), with $Ca_V3.2$ (N = 9), or with $Ca_V3.1$ (N = 10) activated by a train of CA1 action potential waveforms as command voltages. Dots (right) represent averaged $I_{CaV3.3}$ (top), $I_{CaV3.1}$ and $I_{CaV3.2}$ (bottom) normalized for it first spike as a function of time for each experiment **(C)** Dots represent averaged $I_{CaV3.1-3}$ normalized for it first spike as a function of time for each –D5R (N = 8) and + D5R (N = 5) conditions. Extra sum-of-square F test. F = 5.828 (DFn = 3, DFd = 122), *P* = 0.0009. Dash lines represent the single exponential function fitted for each Ca_V3 subtype shown in panel B.

A

B

C

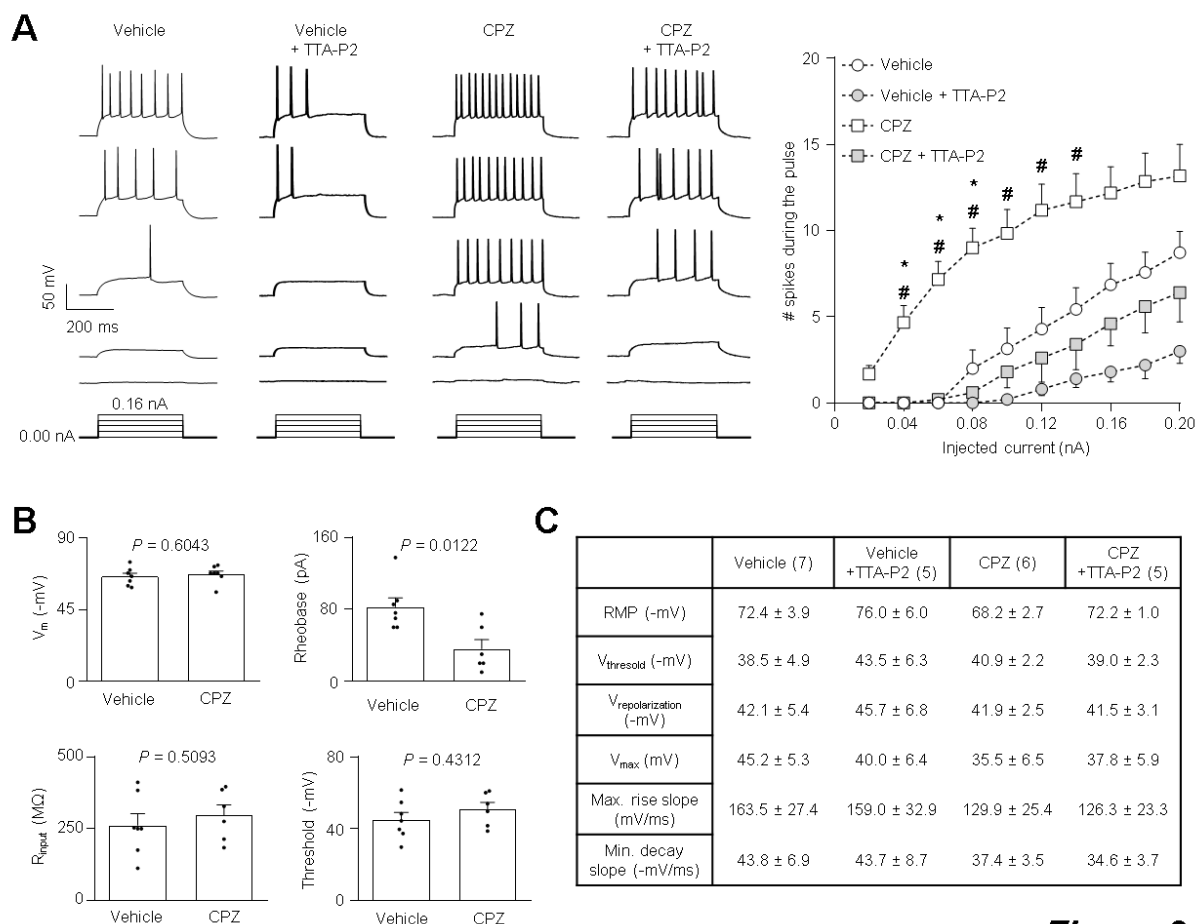|	Vehicle (7)	Vehicle +TTA-P2 (5)	CPZ (6)	CPZ +TTA-P2 (5)
RMP (-mV)	72.4 ± 3.9	76.0 ± 6.0	68.2 ± 2.7	72.2 ± 1.0
$V_{thresold}$ (-mV)	38.5 ± 4.9	43.5 ± 6.3	40.9 ± 2.2	39.0 ± 2.3
$V_{repolarization}$ (-mV)	42.1 ± 5.4	45.7 ± 6.8	41.9 ± 2.5	41.5 ± 3.1
V_{max} (mV)	45.2 ± 5.3	40.0 ± 6.4	35.5 ± 6.5	37.8 ± 5.9
Max. rise slope (mV/ms)	163.5 ± 27.4	159.0 ± 32.9	129.9 ± 25.4	126.3 ± 23.3
Min. decay slope (-mV/ms)	43.8 ± 6.9	43.7 ± 8.7	37.4 ± 3.5	34.6 ± 3.7

Figure 9

Figure 9. (A) Representative traces of voltage response (left) registered with a pulse from 0.00 nA to 0.16 nA in CA1 pyramidal neurons of mice hippocampus treated i.p. with vehicle with (N = 5, 4 animals) or without TTA-P2 (N = 7, 4 animals), or treated i.p. with chlorpromazine (CPZ) with (N = 5, 3 animals) or without TTA-P2 (N = 6, 3 animals) acute application. Dots (right) represent averaged number (#) of spikes during the pulse of current for each condition (injected current from 0.00 to 0.20 nA for 400 ms). Statistical significance was evaluated by Kruskal-Wallis and Dunn's post-test where * indicates differences between vehicle and CPZ, and # indicates differences between CPZ and CPZ + TTA-P2. **(B)** Bars represent the averaged resting membrane potential (V_m), rheobase, input resistance and action potential threshold in CA1 pyramidal neurons of mice hippocampus treated i.p. with vehicle (N = 7, 4 animals) or CPZ (N = 6, 3 animals). CPZ; 1mg/kg. TTA-P2; 1 µM. Statistical significance was evaluated by Mann-Whitney test. **(C)** Table shows the average RMP (resting membrane potential), V_{thre} (threshold membrane potential), $V_{repolarization}$ (repolarization membrane potential), Vmax (maximal voltage peak of the action potential), max. rise slope (maximum rise slope) and min. decay slope (minimum decay slope) values obtained from phase plot analysis of the first action potential (injected current 0.14 nA) for each conditions.

Statistical significance was evaluated by Kruskal-Wallis and Dunn's post-test and we didn´t find significant differences between all the conditions.

Figure 10. Simulations of the firing pattern in a model of hippocampal CA1 pyramidal neuron under different conditions: I_{CaV3} (38 %), I_{CaV3} (100 %) and I_{CaV3} (168 %). Examples of voltage traces obtained with the current stimulus steps from 0.5 to 1.0 nA into the virtual soma. Graph in the right represents the number (#) of spikes during the current stimuli at different percentage of I_{CaV3}.